

Supporting Information
Synthesis and Reactivity of a Low-Coordinate Iron(II) Hydride Complex:
Applications in Catalytic Hydrodefluorination

Nicholas M. Hein, Fraser S. Pick, and Michael D. Fryzuk*

Department of Chemistry
The University of British Columbia
2036 Main Mall
Vancouver, BC, CANADA
V6T 1Z1

Contents:

X-ray Crystallographic Data and Collection Parameters.....	S2
Solid-State Molecular Structures.....	S9
¹ H NMR Characterization for Synthesized Complexes.....	S14
Experimental NMR Spectra.....	S20
Additional Kinetic Data.....	S50

X-ray Crystallographic Data and Collection Parameters

Table S1: Crystal data and structure refinement for **2**

Identification code	mf1263	
Empirical formula	$C_{38.5}H_{59}FeN_2P$	
Formula weight	636.69	
Temperature	90K	
Crystal size	$0.46 \times 0.45 \times 0.11 \text{ mm}^3$	
Radiation	MoK α ($\lambda = 0.71073 \text{ \AA}$)	
Crystal system	monoclinic	
Space group	C2/c	
Unit cell dimensions	$a=27.732(3) \text{ \AA}$	$\alpha=90^\circ$
	$b=14.1554(13) \text{ \AA}$	$\beta=110.078(2)^\circ$
	$c=19.4207(18) \text{ \AA}$	$\gamma=90^\circ$
Volume	$7160.3(11) \text{ \AA}^3$	
Z	8	
Density (calculated)	1.181 g/cm^3	
Absorption Coefficient	0.494 mm^{-1}	
F(000)	2760.0	
2 θ range for data collection	3.128 to 60.202°	
Index ranges	$-35 \leq h \leq 39, -19 \leq k \leq 19, -26 \leq l \leq 27$	
Reflections collected	76880	
Independent reflections	10512 [$R_{\text{int}} = 0.0243, R_{\text{sigma}} = 0.0160$]	
Data/restraints/parameters	10512/447/455	
Completeness to θ	99.8%	
Goodness-of-fit on F^2	1.032	
Final R indexes [$I \geq 2\sigma(I)$]	$R_1 = 0.0317, wR_2 = 0.0762$	
Final R indexes [all data]	$R_1 = 0.0393, wR_2 = 0.0814$	
Largest diff. peak/hole	$0.64/-0.42 \text{ e\AA}^{-3}$	

Table S2: Crystal data and structure refinement for **3**

Identification code	mf1206	
Empirical formula	$C_{39}H_{66}BFeN_2P$	
Formula weight	660.56	
Temperature	90K	
Crystal size	$0.37 \times 0.21 \times 0.16 \text{ mm}^3$	
Radiation	MoK α ($\lambda = 0.71073 \text{ \AA}$)	
Crystal system	monoclinic	
Space group	P2 ₁ /c	
Unit cell dimensions	$a=16.9333(7) \text{ \AA}$	$\alpha=90^\circ$
	$b=11.7516(5) \text{ \AA}$	$\beta=100.5590(10)^\circ$
	$c=20.0066(7) \text{ \AA}$	$\gamma=90^\circ$
Volume	$3913.8(3) \text{ \AA}^3$	
Z	4	
Density (calculated)	1.121 g/cm^3	
Absorption Coefficient	0.453 mm^{-1}	
F(000)	1440.0	
2 θ range for data collection	4.038 to 50.136°	
Index ranges	$-20 \leq h \leq 17$, $-12 \leq k \leq 14$, $-23 \leq l \leq 22$	
Reflections collected	29547	
Independent reflections	6921 [$R_{\text{int}} = 0.0605$, $R_{\text{sigma}} = 0.0656$]	
Data/restraints/parameters	6921/0/419	
Completeness to θ	99.7%	
Goodness-of-fit on F^2	1.011	
Final R indexes [$I \geq 2\sigma(I)$]	$R_1 = 0.0501$, $wR_2 = 0.1034$	
Final R indexes [all data]	$R_1 = 0.0810$, $wR_2 = 0.1146$	
Largest diff. peak/hole	$0.46/-0.49 \text{ e\AA}^{-3}$	

Table S3: Crystal data and structure refinement for **4**

Identification code	mf1296	
Empirical formula	$C_{37}H_{56.67}FeN_2P$	
Formula weight	616.33	
Temperature	90K	
Crystal size	$0.75 \times 0.75 \times 0.55 \text{ mm}^3$	
Radiation	MoK α ($\lambda = 0.71073 \text{ \AA}$)	
Crystal system	Orthorhombic	
Space group	Pbca	
Unit cell dimensions	$a=19.4365(19) \text{ \AA}$	$\alpha=90^\circ$
	$b=17.908(2) \text{ \AA}$	$\beta=90^\circ$
	$c=19.954(2) \text{ \AA}$	$\gamma=90^\circ$
Volume	$6945.5(13) \text{ \AA}^3$	
Z	8	
Density (calculated)	1.179 g/cm^3	
Absorption Coefficient	0.507 mm^{-1}	
F(000)	2669.0	
2 θ range for data collection	3.706 to 59.222°	
Index ranges	$-27 \leq h \leq 26$, $-24 \leq k \leq 23$, $-27 \leq l \leq 27$	
Reflections collected	76719	
Independent reflections	9766 [$R_{\text{int}} = 0.0354$, $R_{\text{sigma}} = 0.0205$]	
Data/restraints/parameters	9766/0/436	
Completeness to θ	99.9%	
Goodness-of-fit on F^2	1.027	
Final R indexes [$I \geq 2\sigma(I)$]	$R_1 = 0.0309$, $wR_2 = 0.0840$	
Final R indexes [all data]	$R_1 = 0.0379$, $wR_2 = 0.0889$	
Largest diff. peak/hole	$0.42/-0.30 \text{ e\AA}^{-3}$	

Table S4: Crystal data and structure refinement for **5**

Identification code	mf1307	
Empirical formula	$C_{47}H_{65}FeN_4P$	
Formula weight	772.85	
Temperature	90K	
Crystal size	$0.28 \times 0.16 \times 0.16 \text{ mm}^3$	
Radiation	MoK α ($\lambda = 0.71073 \text{ \AA}$)	
Crystal system	Orthorhombic	
Space group	P2 ₁ 2 ₁ 2 ₁	
Unit cell dimensions	a=11.4731(10) \AA	$\alpha=90^\circ$
	b=19.0046(18) \AA	$\beta=90^\circ$
	c=20.1296(17) \AA	$\gamma=90^\circ$
Volume	4389.1(7) \AA^3	
Z	4	
Density (calculated)	1.170 g/cm ³	
Absorption Coefficient	0.416 mm ⁻¹	
F(000)	1664.0	
2 θ range for data collection	4.086 to 55.73°	
Index ranges	$-14 \leq h \leq 14, -24 \leq k \leq 24, -26 \leq l \leq 26$	
Reflections collected	64774	
Independent reflections	10218 [$R_{\text{int}} = 0.0931, R_{\text{sigma}} = 0.0757$]	
Data/restraints/parameters	10218/0/490	
Completeness to θ	98.1%	
Goodness-of-fit on F^2	1.015	
Final R indexes [$I \geq 2\sigma(I)$]	$R_1 = 0.0535, wR_2 = 0.1355$	
Final R indexes [all data]	$R_1 = 0.0643, wR_2 = 0.1405$	
Largest diff. peak/hole	0.68/-0.32 e \AA^{-3}	

Table S5: Crystal data and structure refinement for **6**

Identification code	mf1302	
Empirical formula	$C_{41}H_{65}FeN_2P$	
Formula weight	672.77	
Temperature	90K	
Crystal size	$0.42 \times 0.34 \times 0.33 \text{ mm}^3$	
Radiation	MoK α ($\lambda = 0.71073 \text{ \AA}$)	
Crystal system	Triclinic	
Space group	P-1	
Unit cell dimensions	$a=10.5433(8) \text{ \AA}$	$\alpha=95.482(4)^\circ$
	$b=11.8988(9) \text{ \AA}$	$\beta=100.646(4)^\circ$
	$c=16.9020(12) \text{ \AA}$	$\gamma=108.968(4)^\circ$
Volume	$1942.9(3) \text{ \AA}^3$	
Z	2	
Density (calculated)	1.150 g/cm^3	
Absorption Coefficient	0.458 mm^{-1}	
F(000)	732.0	
2 θ range for data collection	3.672 to 55.088°	
Index ranges	$-13 \leq h \leq 13$, $-15 \leq k \leq 15$, $-21 \leq l \leq 21$	
Reflections collected	34076	
Independent reflections	8917 [$R_{\text{int}} = 0.0423$, $R_{\text{sigma}} = 0.0403$]	
Data/restraints/parameters	8917/0/420	
Completeness to θ	99.9%	
Goodness-of-fit on F^2	1.051	
Final R indexes [$I \geq 2\sigma(I)$]	$R_1 = 0.0443$, $wR_2 = 0.1188$	
Final R indexes [all data]	$R_1 = 0.0575$, $wR_2 = 0.1277$	
Largest diff. peak/hole	$0.88/-0.54 \text{ e\AA}^{-3}$	

Table S6: Crystal data and structure refinement for **7**

Identification code	mf1214	
Empirical formula	$C_{32.33}H_{49.33}Fe_{0.67}N_{3.33}P_{0.67}$	
Formula weight	542.63	
Temperature	100K	
Crystal size	$0.3 \times 0.17 \times 0.07 \text{ mm}^3$	
Radiation	MoK α ($\lambda = 0.71073 \text{ \AA}$)	
Crystal system	Monoclinic	
Space group	P2 ₁ /n	
Unit cell dimensions	$a=10.4848(10) \text{ \AA}$	$\alpha=90^\circ$
	$b=24.631(3) \text{ \AA}$	$\beta=98.444(4)^\circ$
	$c=17.7095(19) \text{ \AA}$	$\gamma=90^\circ$
Volume	$4523.9(8) \text{ \AA}^3$	
Z	6	
Density (calculated)	1.195 g/cm^3	
Absorption Coefficient	0.407 mm^{-1}	
F(000)	1764.0	
2 θ range for data collection	4.26 to 53.61°	
Index ranges	$-13 \leq h \leq 9$, $-31 \leq k \leq 30$, $-22 \leq l \leq 18$	
Reflections collected	28699	
Independent reflections	9560 [$R_{\text{int}} = 0.0604$, $R_{\text{sigma}} = 0.0799$]	
Data/restraints/parameters	9560/0/531	
Completeness to θ	98.7%	
Goodness-of-fit on F^2	1.052	
Final R indexes [$I \geq 2\sigma(I)$]	$R_1 = 0.0452$, $wR_2 = 0.1076$	
Final R indexes [all data]	$R_1 = 0.0716$, $wR_2 = 0.1177$	
Largest diff. peak/hole	$0.48/-0.34 \text{ e\AA}^{-3}$	

Table S7: Crystal data and structure refinement for **8**

Identification code	mf1248_sq	
Empirical formula	$C_{73.5}H_{112}F_2Fe_2N_4P_2$	
Formula weight	1263.30	
Temperature	90K	
Crystal size	$0.14 \times 0.12 \times 0.06 \text{ mm}^3$	
Radiation	MoK α ($\lambda = 0.71073 \text{ \AA}$)	
Crystal system	Monoclinic	
Space group	$P2_1/c$	
Unit cell dimensions	$a=20.445(6) \text{ \AA}$	$\alpha=90^\circ$
	$b=13.612(4) \text{ \AA}$	$\beta=92.564(9)^\circ$
	$c=26.186(9) \text{ \AA}$	$\gamma=90^\circ$
Volume	$7280(4) \text{ \AA}^3$	
Z	4	
Density (calculated)	1.153 g/cm^3	
Absorption Coefficient	0.489 mm^{-1}	
F(000)	2724.0	
2 θ range for data collection	1.994 to 44.786°	
Index ranges	$-21 \leq h \leq 21, 0 \leq k \leq 14, 0 \leq l \leq 28$	
Reflections collected	9266	
Independent reflections	9266 [$R_{\text{sigma}} = 0.1002$]	
Data/restraints/parameters	9266/735/802	
Completeness to θ	97.9%	
Goodness-of-fit on F^2	1.031	
Final R indexes [$I \geq 2\sigma(I)$]	$R_1 = 0.0613, wR_2 = 0.1311$	
Final R indexes [all data]	$R_1 = 0.0948, wR_2 = 0.1454$	
Largest diff. peak/hole	$0.53/-0.48 \text{ e\AA}^{-3}$	

Solid State Molecular Structures

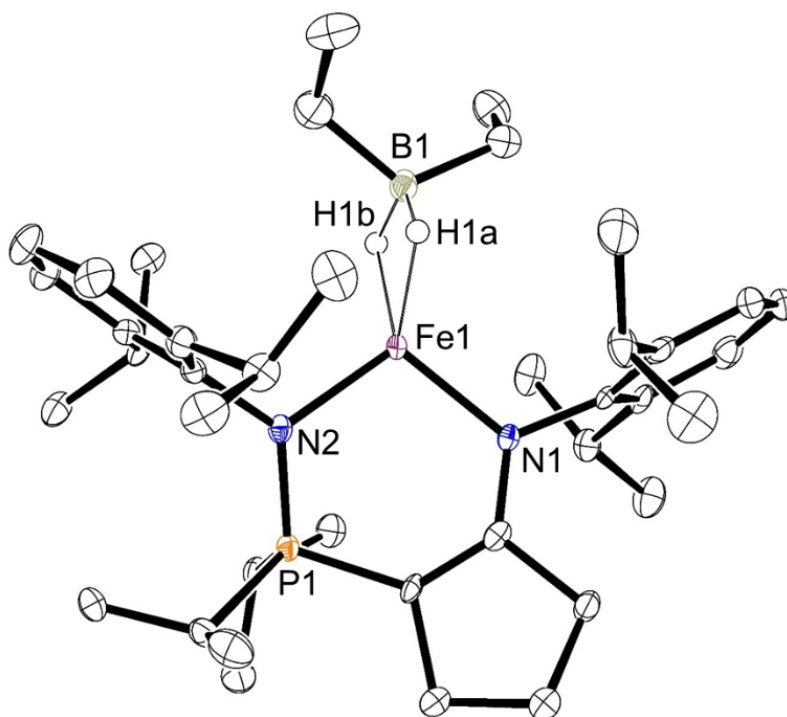


Figure S1: ORTEP drawing of the solid-state molecular structure of **3** (ellipsoids at 50% probability level). All hydrogen atoms except those bonded to iron have been omitted for clarity. Selected bond lengths (Å) and angles (deg): Fe1-N1: 1.952(2), Fe1-N2: 1.971(2), P1-N2: 1.632(2), Fe1-H1a: 1.81(3), Fe1-H1b: 1.66(3), N1-Fe1-N2: 105.26(9), and H1a-Fe1-H1b: 59.8(14).

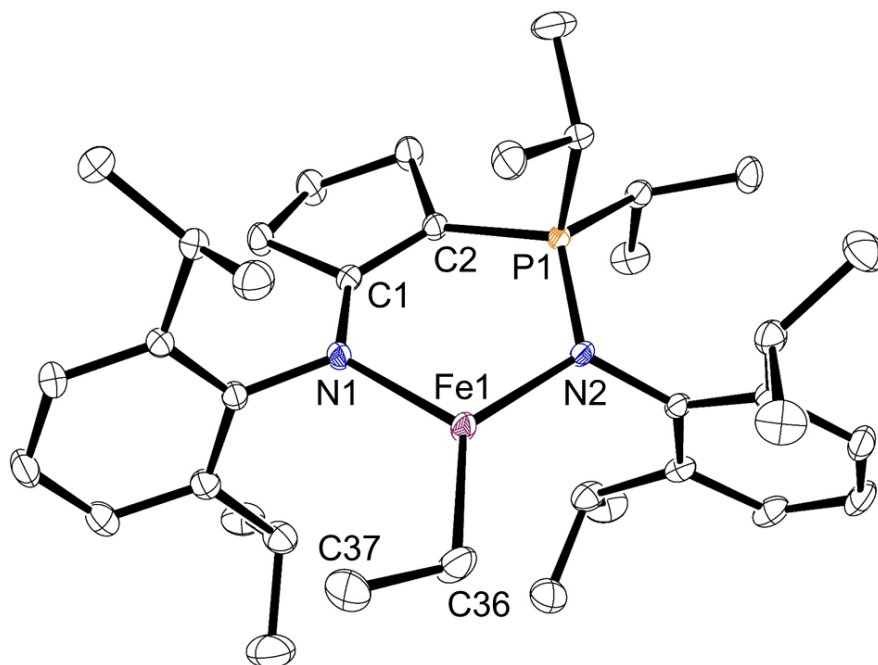


Figure S2: ORTEP drawing of the solid-state molecular structure of **4** (ellipsoids at 50% probability level). All hydrogen atoms have been omitted for clarity. Selected bond lengths (Å) and angles (deg): Fe1-N1: 1.9860(10), Fe1-N2: 2.0072(9), C1-N1: 1.3524(14), C1-C2: 1.3853(15), C2-P1: 1.7564(11), P1-N2: 1.6314(9), Fe1-C36: 2.052(5), C36-C37: 1.481(10), N1-Fe1-N2: 103.44(4), and C37-C36-Fe1: 116.9(4).

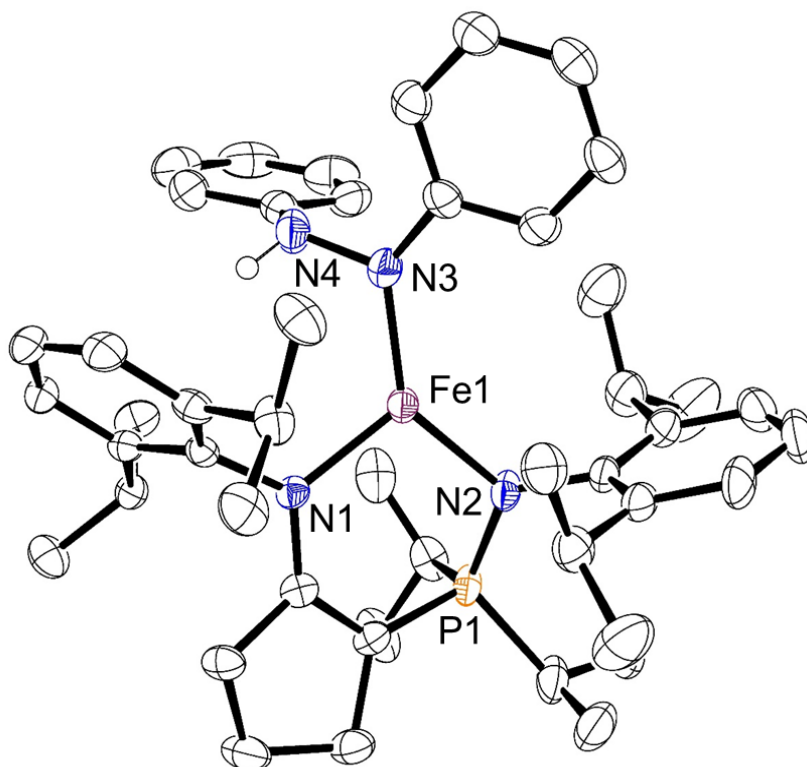


Figure S3: ORTEP drawing of the solid-state molecular structure of **5** (ellipsoids at 50% probability level). All hydrogen atoms except those bonded to N have been omitted for clarity. Selected bond lengths (Å) and angles (deg): Fe1-N1: 1.973(3), Fe1-N2: 1.990(3), N3-N4: 1.429(5), Fe1-N3: 1.934(3), P1-N2: 1.644(4), N1-Fe1-N2: 104.46(14), and Fe1-N3-N4: 115.7(3).

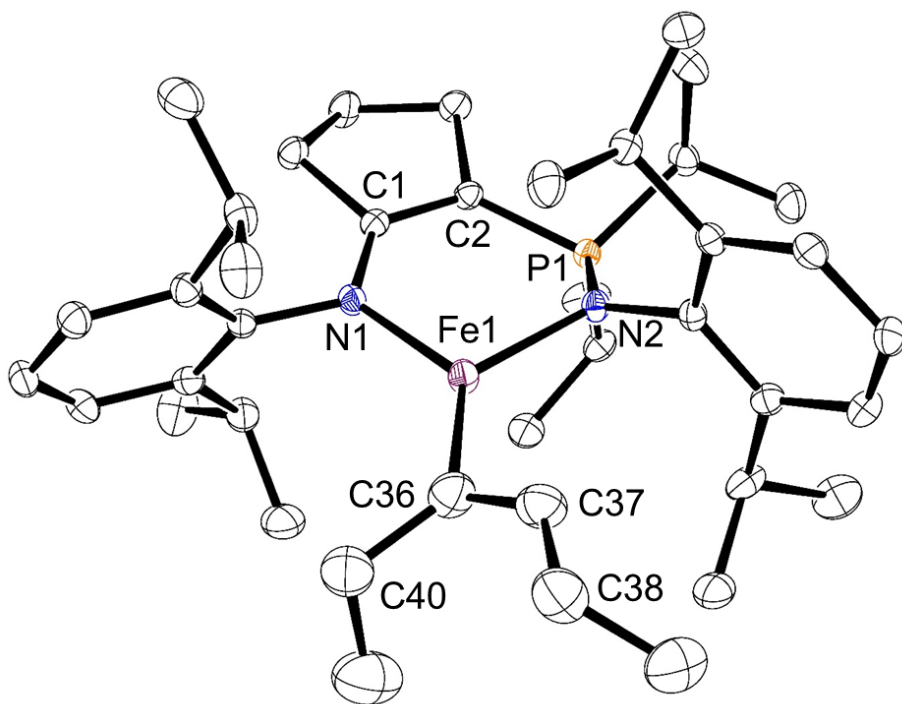


Figure S4: ORTEP drawing of the solid-state molecular structure of **6** (ellipsoids at 50% probability level). All hydrogen atoms have been omitted for clarity. Selected bond lengths (Å) and angles (deg): Fe1-N1: 1.9807(16), Fe1-N2: 2.0081(16), Fe1-C36: 2.016(2), C1-C2: 1.387(3), C1-N1: 1.355(2), C2-P1: 1.7605(19), P1-N2: 1.6295(16), C36-C40: 1.526(4), C36-C37: 1.369(4), C37-C38: 1.502(3), N1-Fe1-N2: 102.02(6), C36-Fe1-N1: 130.40(8), C36-Fe1-N2: 127.31(9), and C40-C36-C37: 120.0(2).

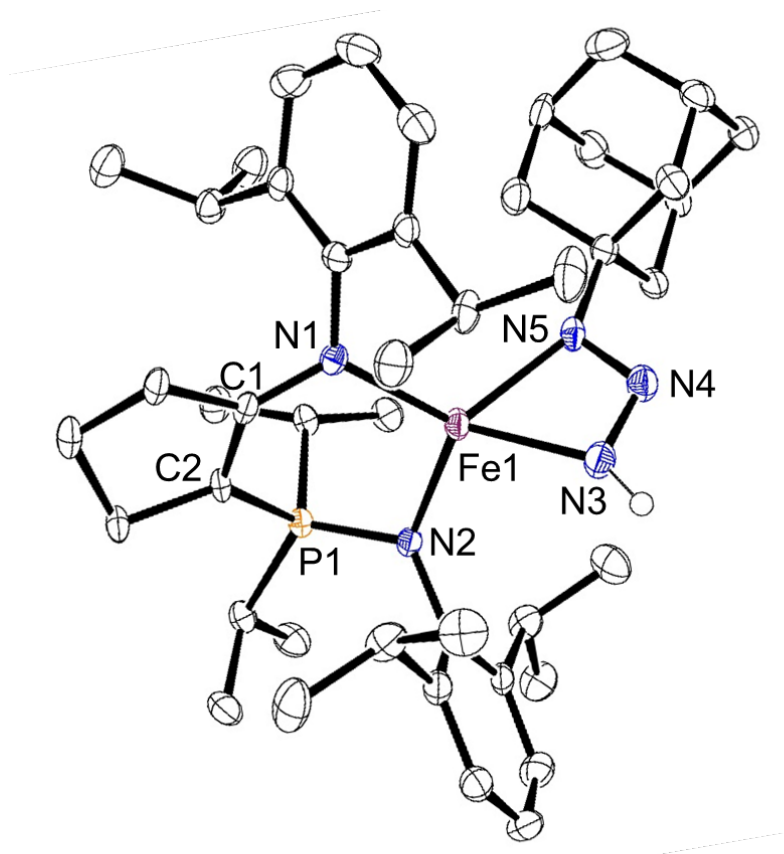


Figure S5: ORTEP drawing of the solid-state molecular structure of **7** (ellipsoids at 50% probability level). All hydrogen atoms except those bonded to N have been omitted for clarity. Selected bond lengths (Å) and angles (deg): Fe1-N1: 2.0170(16), Fe1-N2: 2.0273(17), C1-C2: 1.376(3), C1-N1: 1.369(2), C2-P1: 1.770(2), P1-N2: 1.6263(16), Fe1-N3: 2.1060(17), Fe1-N5: 2.0901(17), N3-N4: 1.321(3), N4-N5: 1.296(2), N1-Fe1-N2: 104.95(7), N3-Fe1-N5: 60.30(7), and N3-N4-N5: 107.26(16).

^1H NMR Characterization for Synthesized Complexes

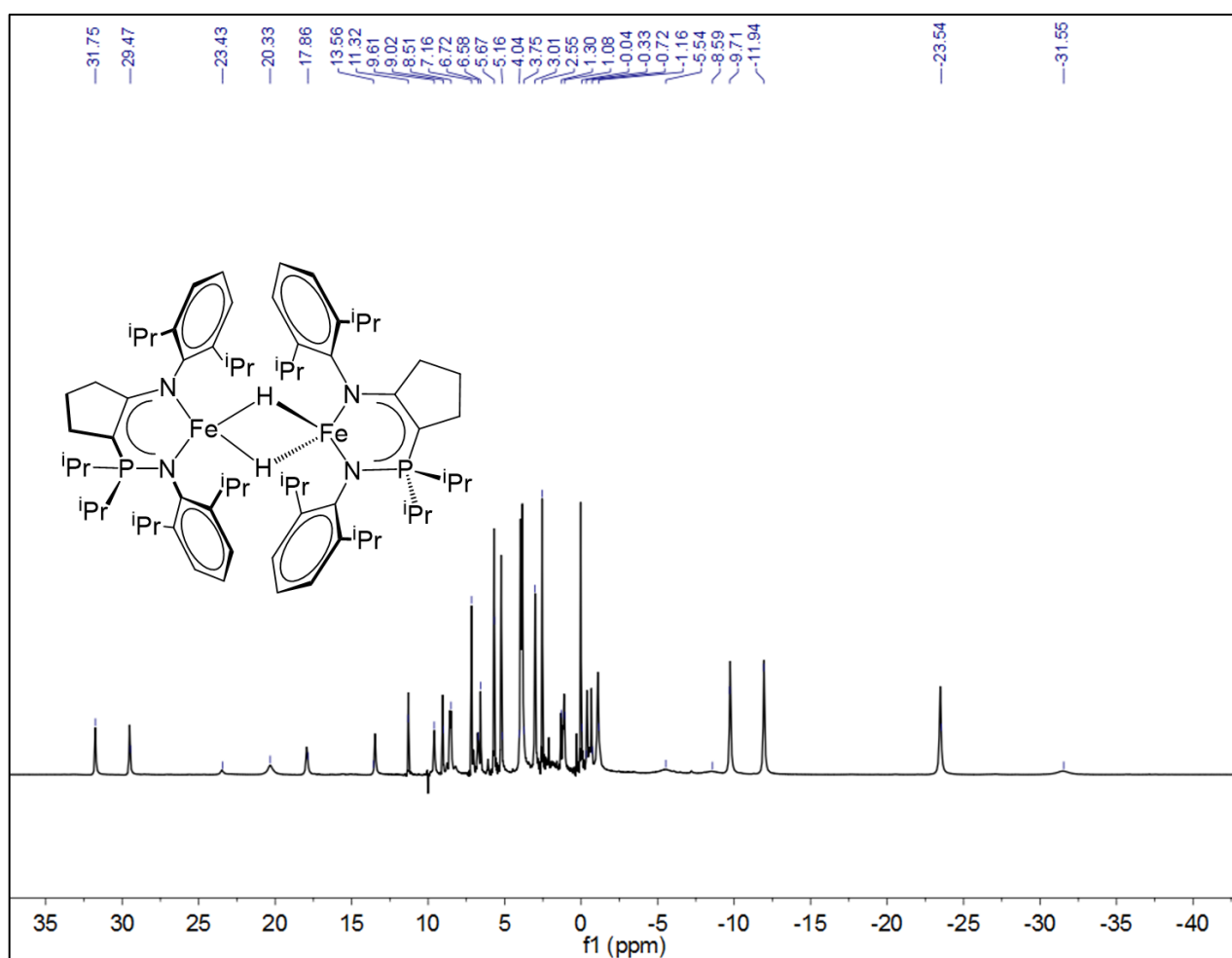


Figure S6: ^1H NMR spectrum for $[(^{\text{CY5}}\text{NpN}^{\text{DIPP,DIPP}})\text{FeH}]_2$ **2** (400 MHz, d_6 -benzene, 25 °C).

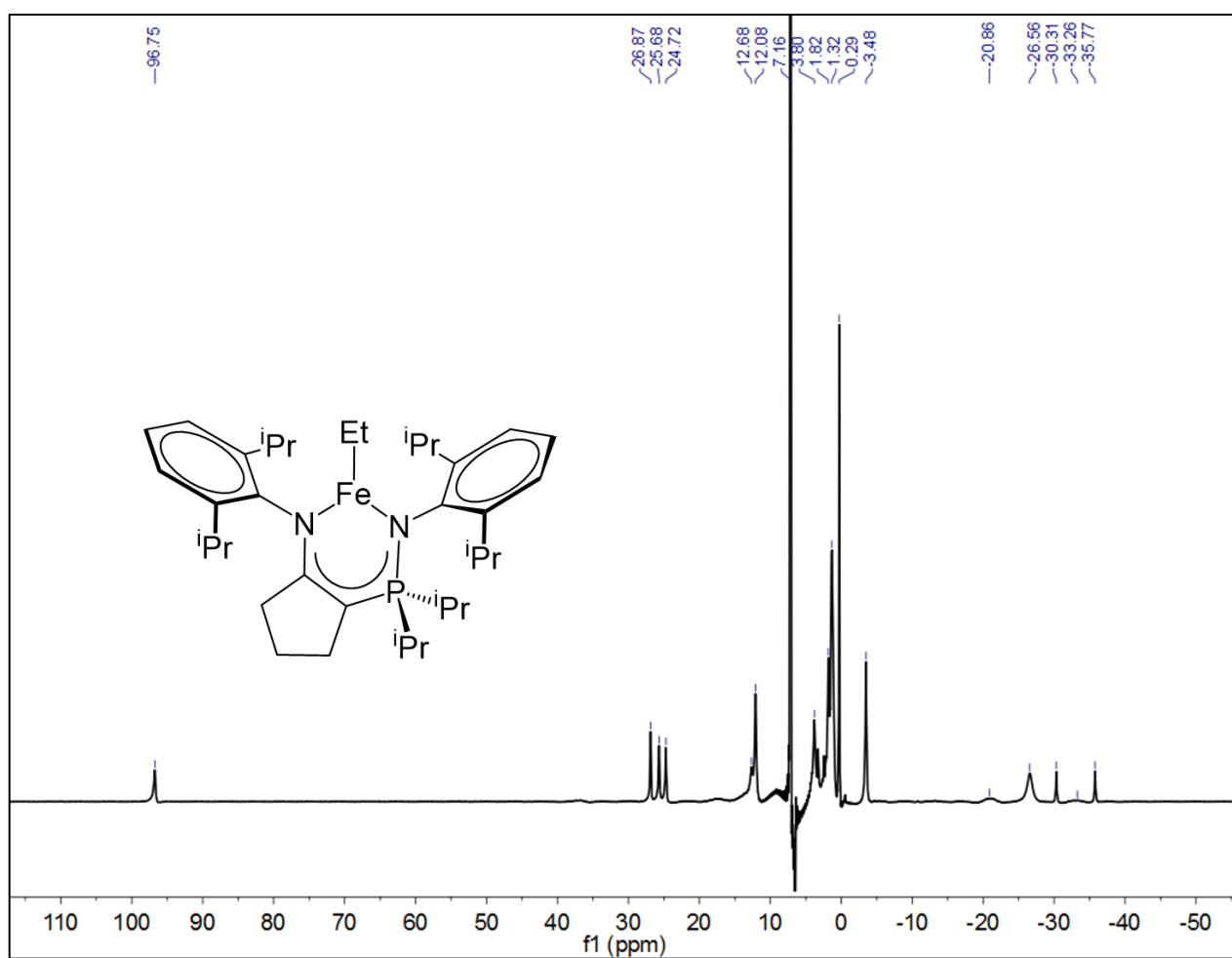


Figure S7: ^1H NMR spectrum for $(^{\text{CY5}}\text{NpN}^{\text{DIPP,DIPP}})\text{FeEt}$ 4 (300 MHz, d_6 -benzene, 25 °C).

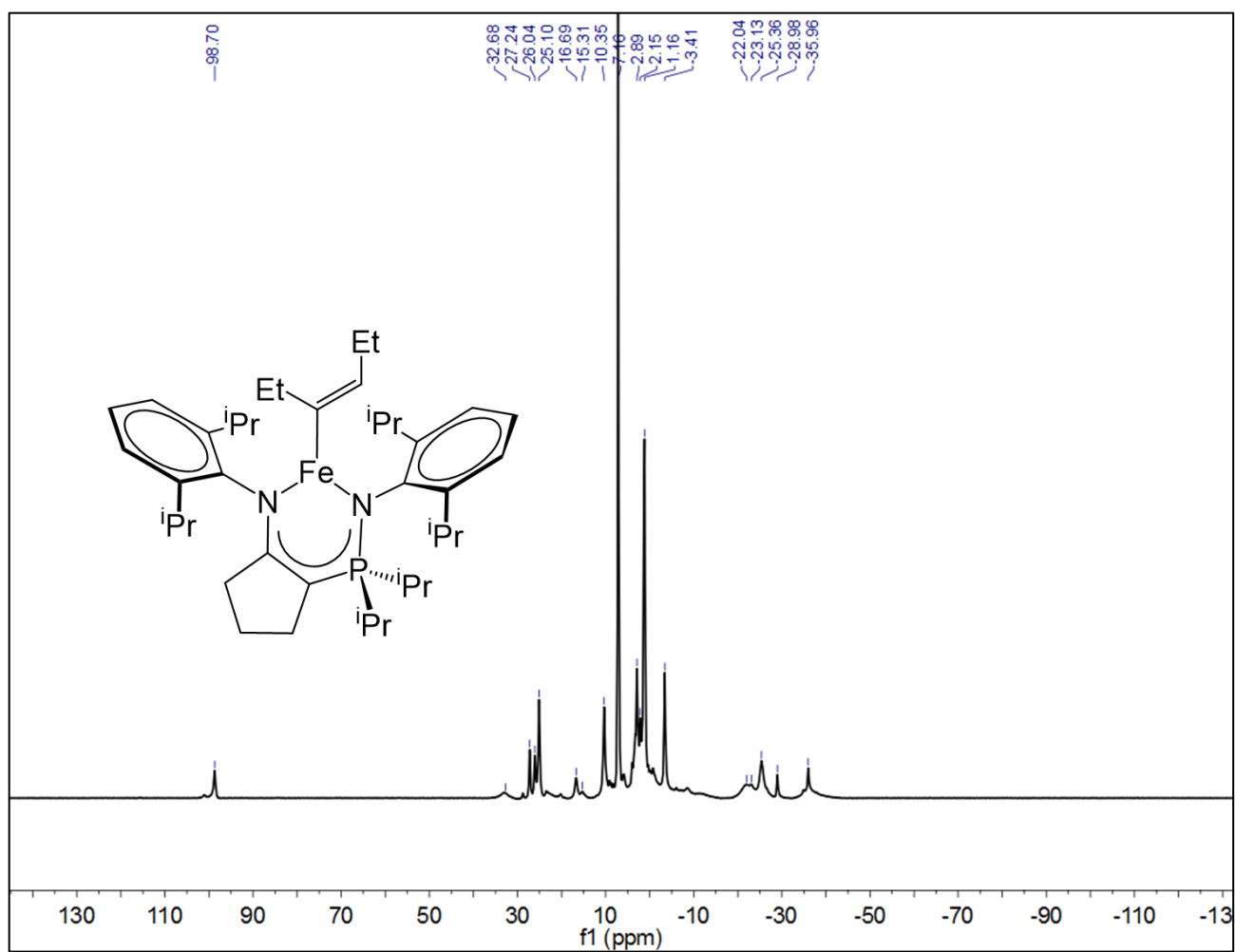


Figure S9: ^1H NMR spectrum for $(\text{CY}^5\text{NpN}^{\text{DIPP,DIPP}})\text{Fe}(\text{3-hexene})$ 6 (300 MHz, d_6 -benzene, 25 °C).

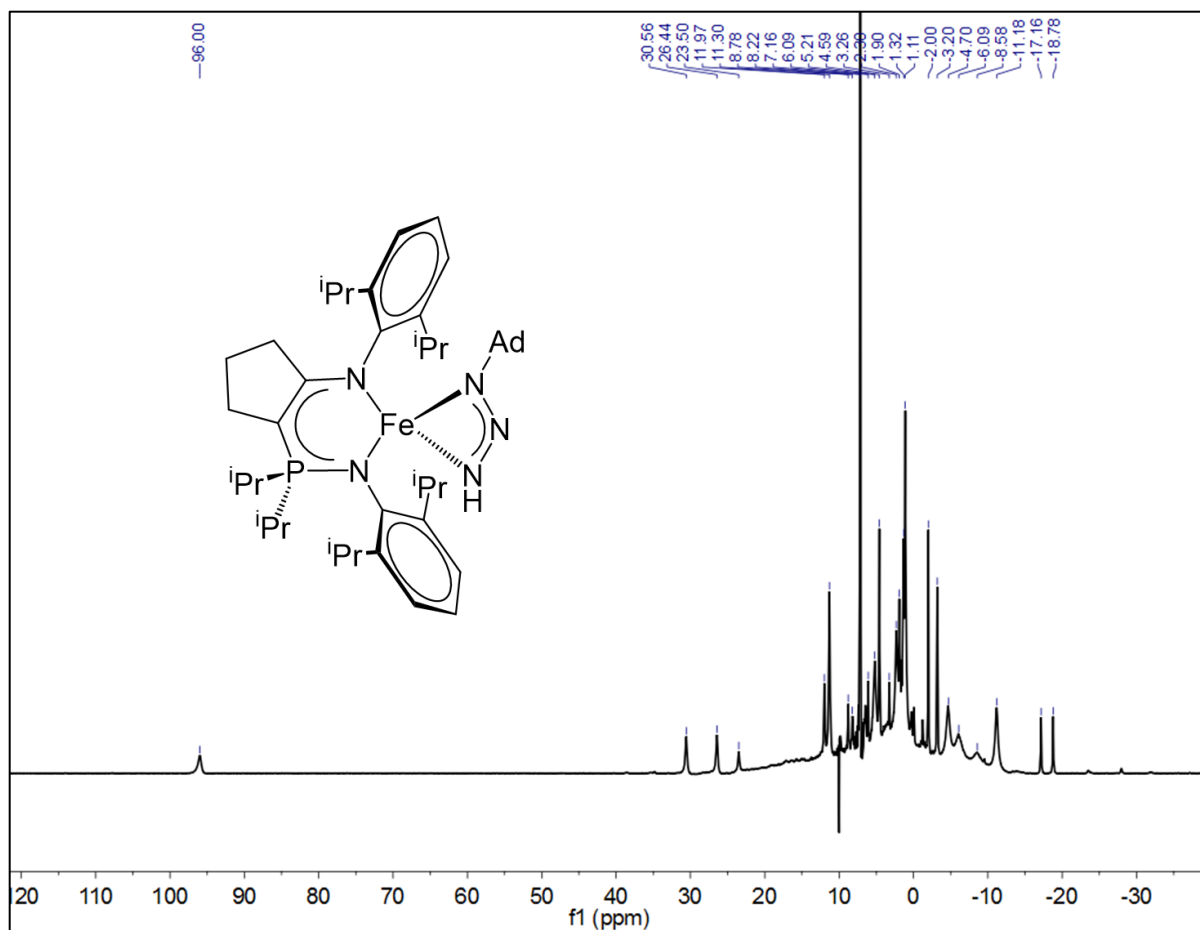


Figure S10: 1H NMR spectrum for $(^{CY5}NpN^{DIPP,DIPP})Fe(\eta^2-HNNAAd)$ 7 (400 MHz, d_6 -benzene, 25 °C).

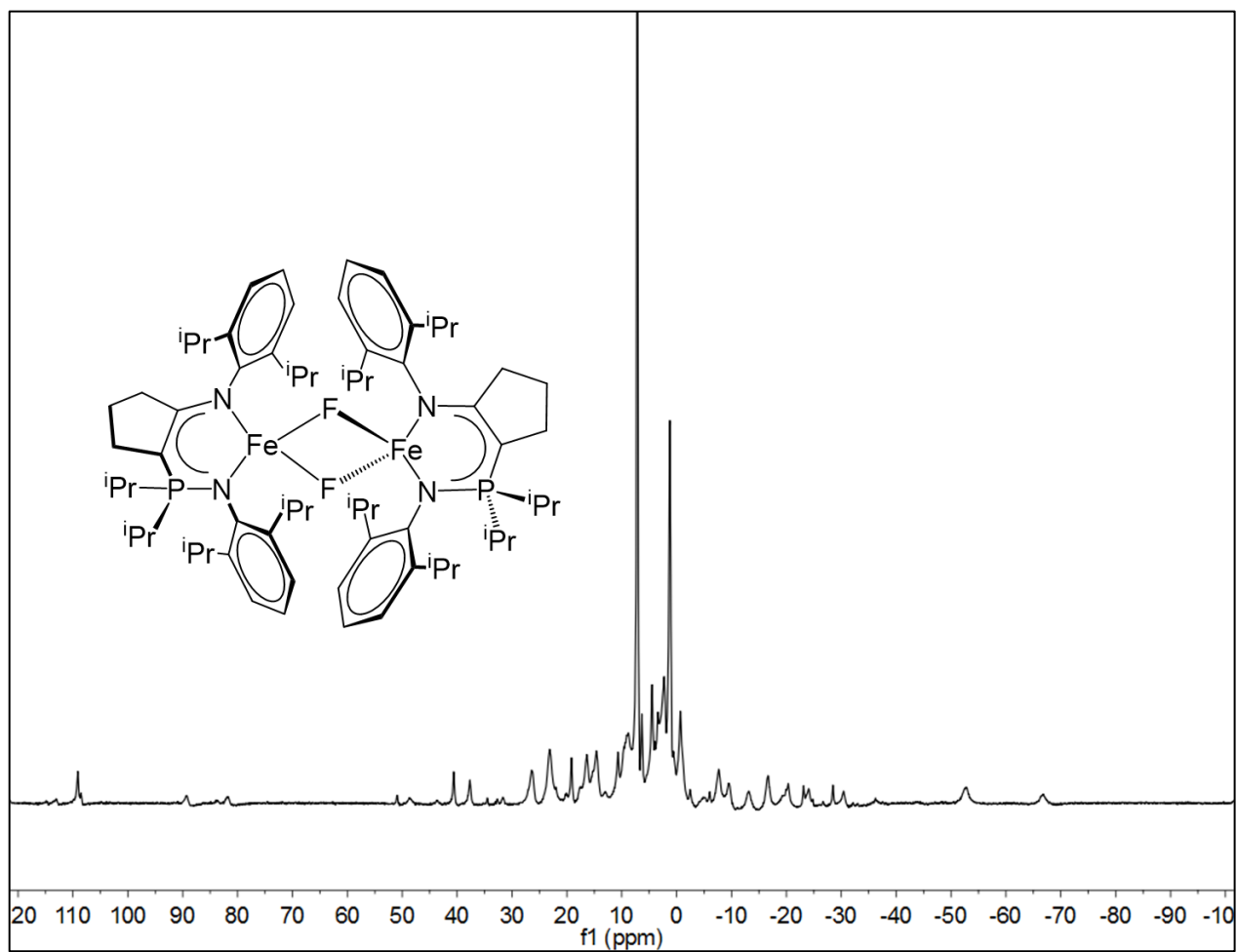


Figure S11: ^1H NMR spectrum for $[(^{\text{CY5}}\text{NpN}^{\text{DIPP,DIPP}})\text{FeF}]_2$ **8** (300 MHz, d_6 -benzene, 25 °C).

Experimental NMR Spectra

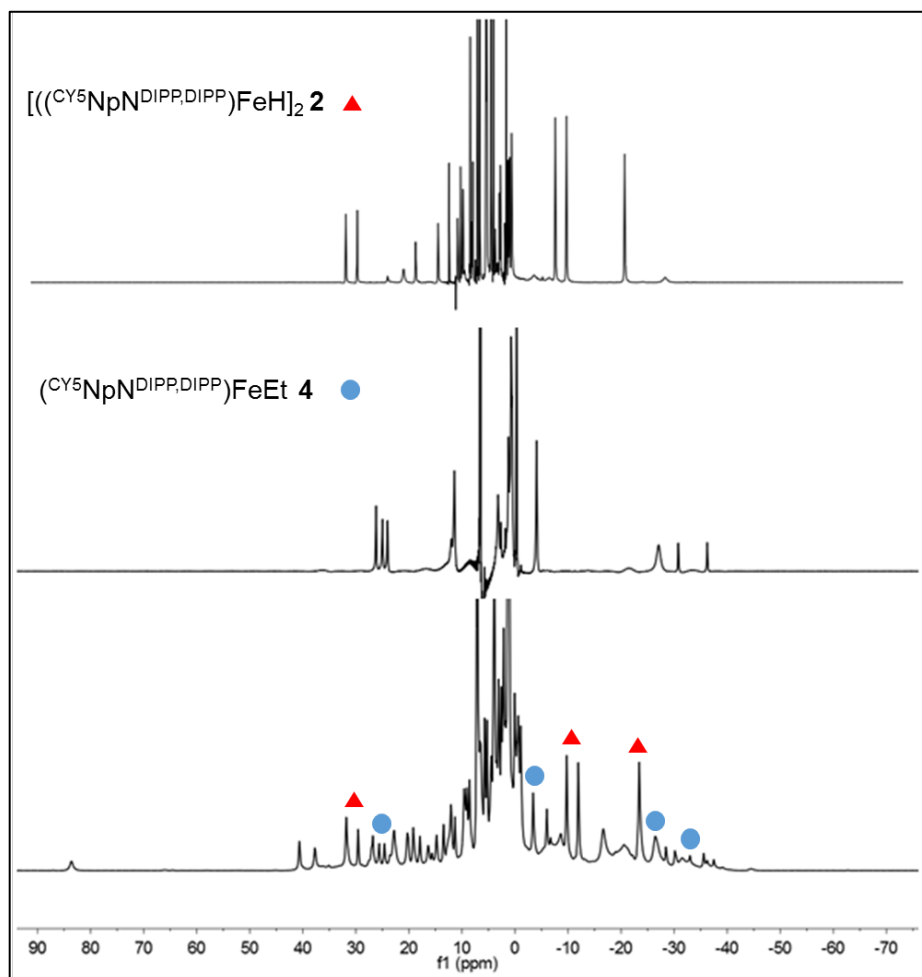


Figure S12: ^1H NMR spectra for $[(\text{CY}^5\text{NpN}^{\text{DIPP,DIPP}})\text{FeH}]_2 \mathbf{2}$ (top), $(\text{CY}^5\text{NpN}^{\text{DIPP,DIPP}})\text{FeEt} \mathbf{4}$ (middle), and the product mixture from which single crystals of $(\text{CY}^5\text{NpN}^{\text{DIPP,DIPP}})\text{FeH}_2\text{BEt}_2 \mathbf{3}$ were grown (bottom). Red triangles for $\mathbf{2}$ and blue circles for $\mathbf{4}$ are used to mark easily discernable signals belonging to their respective compounds in the complicated product mixture shown in the bottom spectrum. All spectra recorded at 300 MHz in d_6 -benzene at 25 °C.

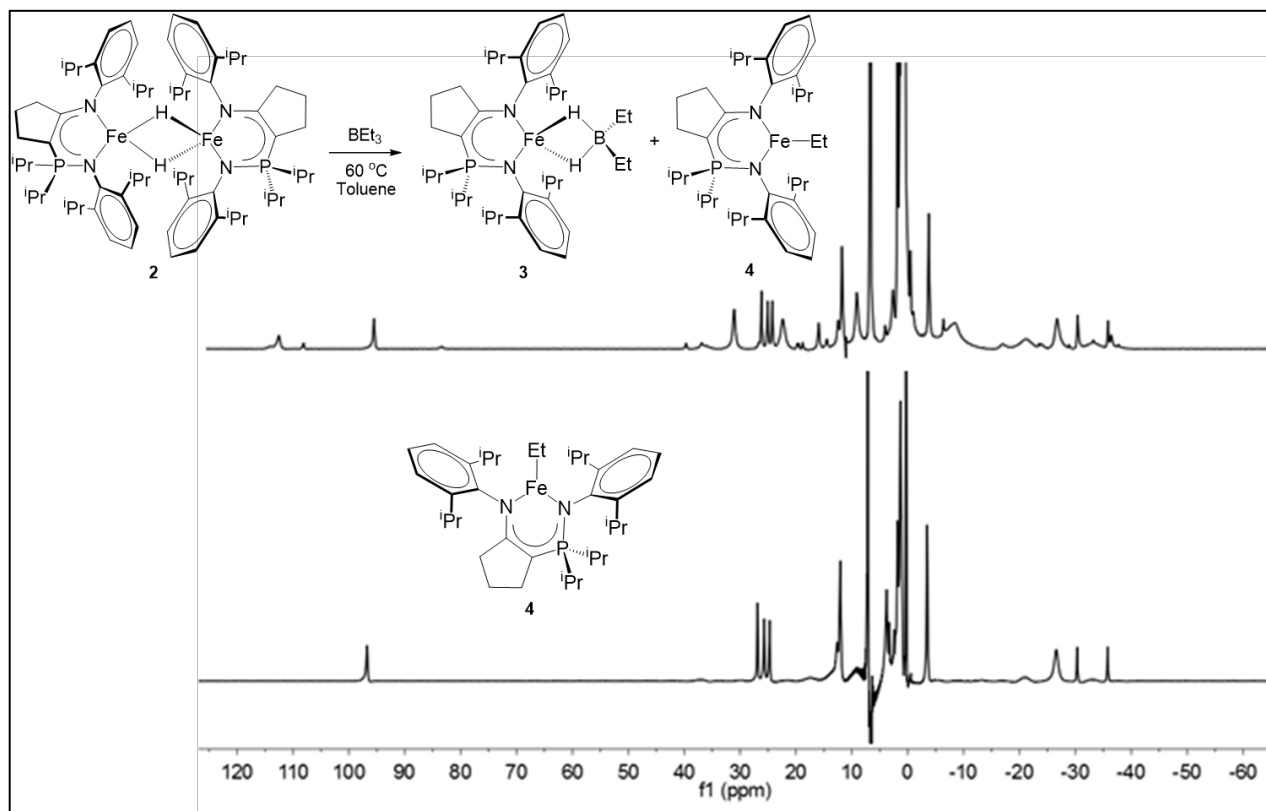


Figure S13: ^1H NMR spectra for the reaction of **2** with BEt_3 at 60°C for 2h (top spectrum, 300 MHz, d_8 -toluene, 25°C), and for complex **4** (bottom spectrum, 300 MHz, d_6 -benzene, 25°C).

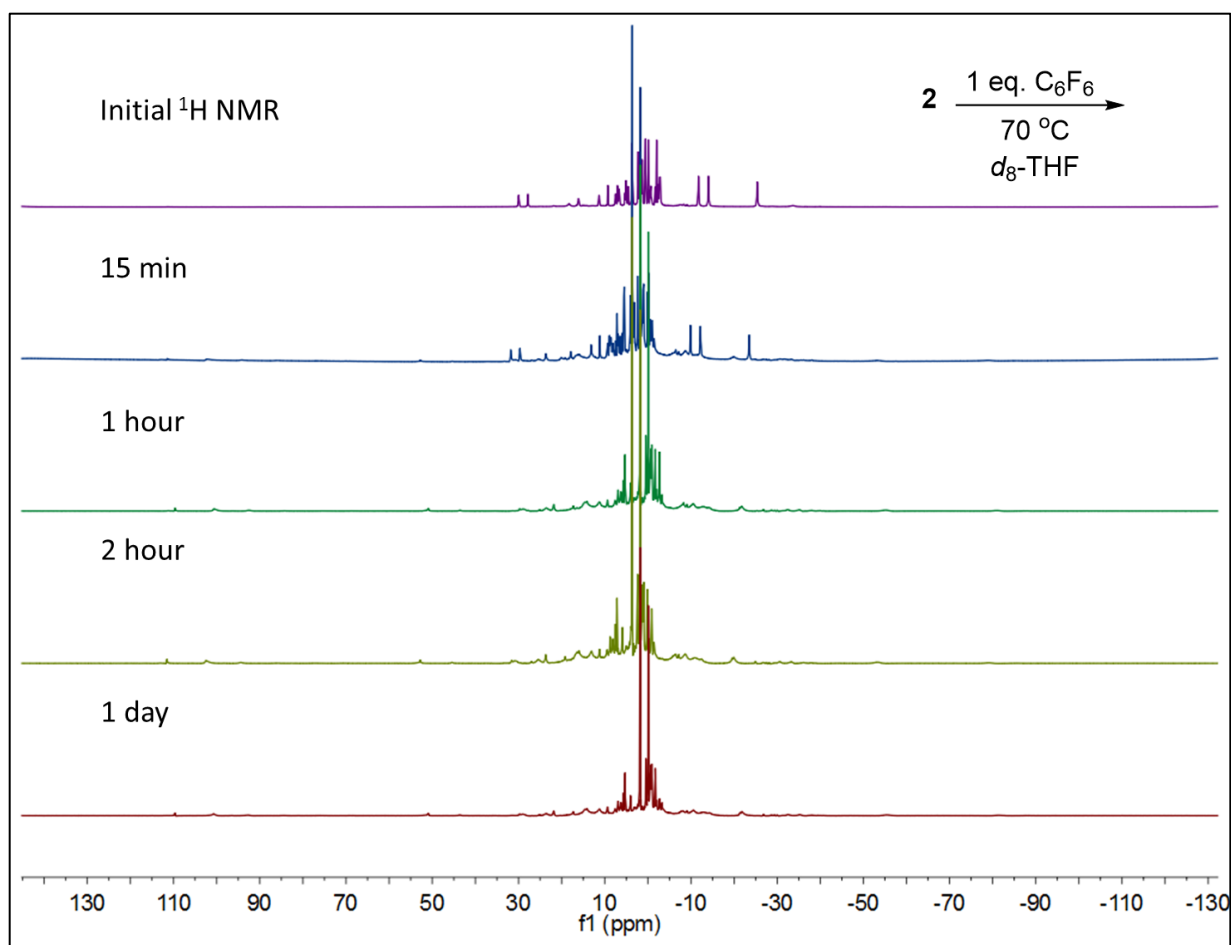


Figure S14: ^1H NMR spectra for the stoichiometric reaction of **2** with C_6F_6 at $70\text{ }^\circ\text{C}$ in $d_8\text{-THF}$. ^1H NMR spectra were collected after 15 minutes, 1 hour, 2 hours, and 1 day. All spectra were collected in $d_8\text{-THF}$ at 300 MHz at $25\text{ }^\circ\text{C}$.

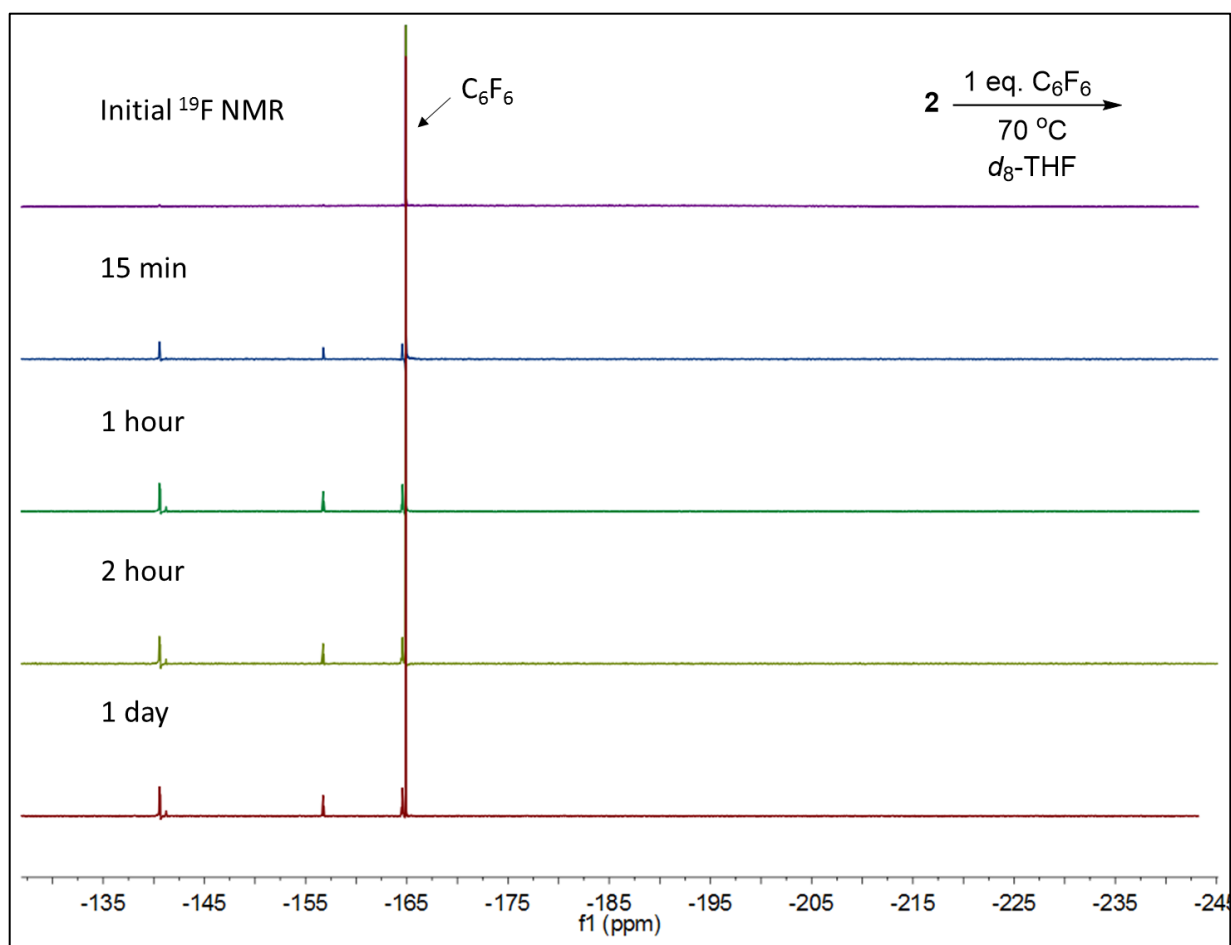


Figure S15: ^{19}F NMR spectra for the stoichiometric reaction of **2** with C_6F_6 at $70\text{ }^\circ\text{C}$ in $d_8\text{-THF}$. ^{19}F NMR spectra were collected after 15 minutes, 1 hour, 2 hours, and 1 day. All spectra were collected in $d_8\text{-THF}$ at 282 MHz at $25\text{ }^\circ\text{C}$.

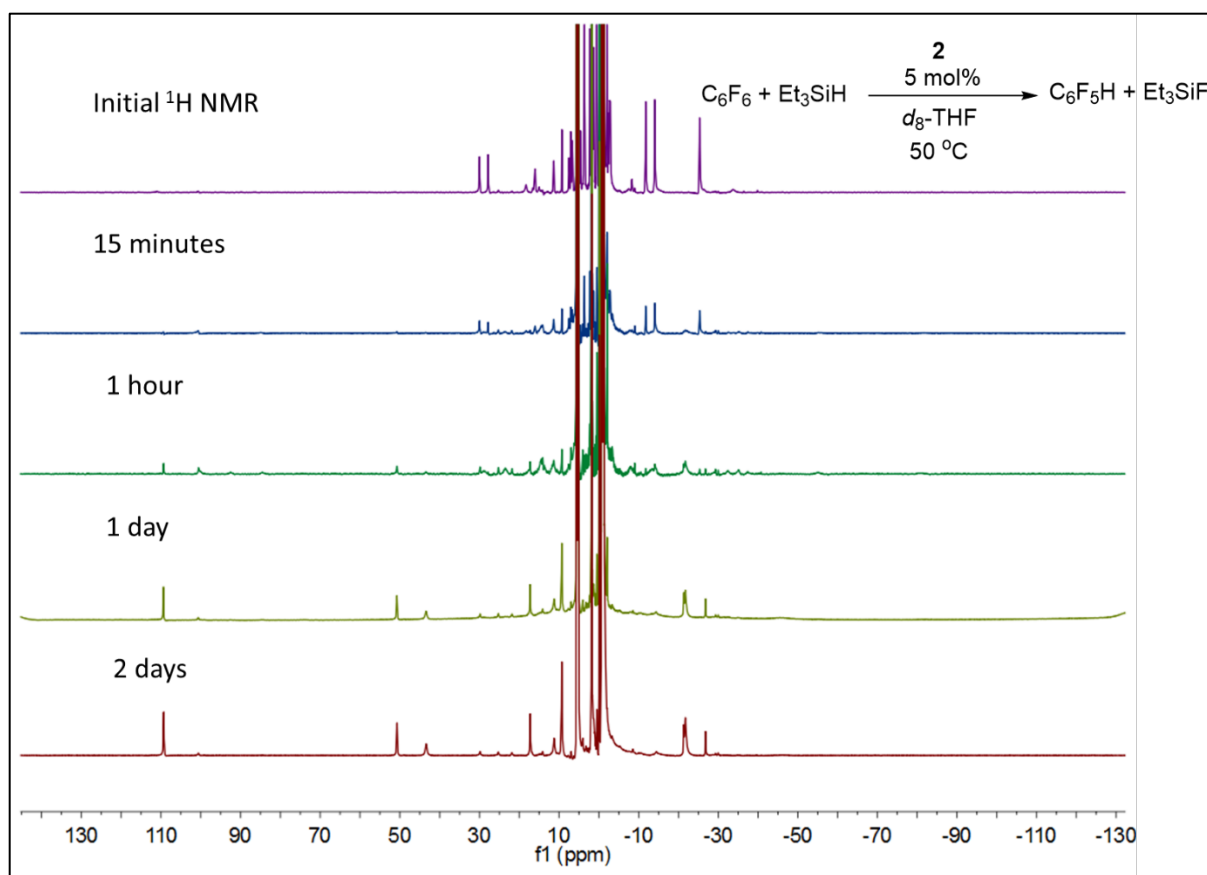


Figure S16: Stacked ^1H NMR spectra for the catalytic monodefluorination of C_6F_6 in the presence of Et_3SiH using **2** as the catalyst at 50°C in $d_8\text{-THF}$. It can be seen that the bridging hydride species **2** is completely consumed after allowing the reaction to proceed for 1 hour. A new paramagnetic species is formed, which is the resting state of the catalyst. All spectra collected in $d_8\text{-THF}$ at 300 MHz at 25°C .

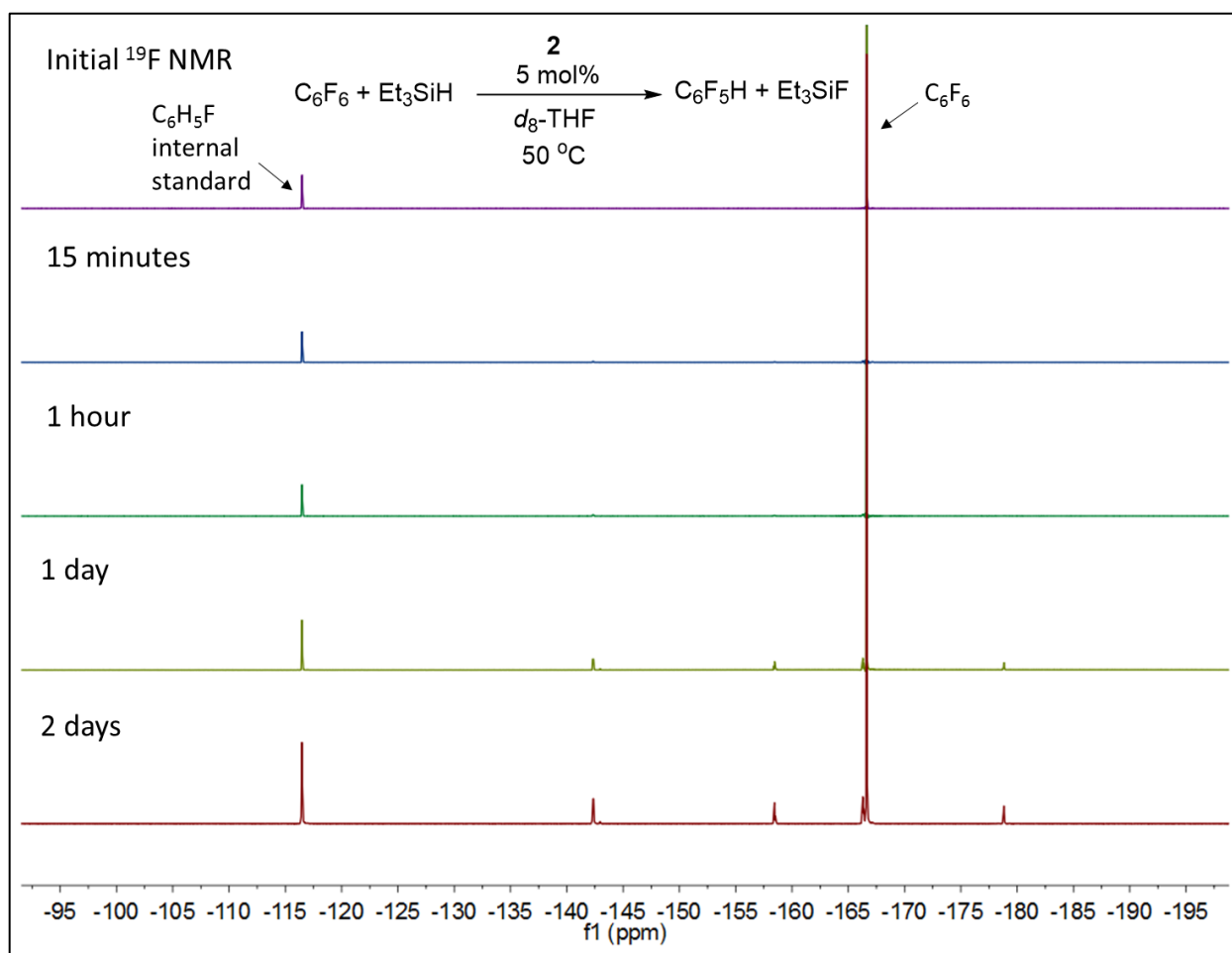


Figure S17: Stacked ^{19}F NMR spectra for the catalytic monodefluorination of C_6F_6 in the presence of Et_3SiH using **2** as the catalyst at $50\text{ }^\circ\text{C}$ in $d_8\text{-THF}$. Fluorobenzene ($\text{C}_6\text{H}_5\text{F}$) is used as the internal standard. ^{19}F resonances corresponding to pentafluorobenzene ($\text{C}_6\text{F}_5\text{H}$) at δ - 139.0, - 155.1, and -163.0 and fluorotriethylsilane at δ -175.5 are observed after 1 day of reactivity. All spectra collected in $d_8\text{-THF}$ at 282 MHz at $25\text{ }^\circ\text{C}$.

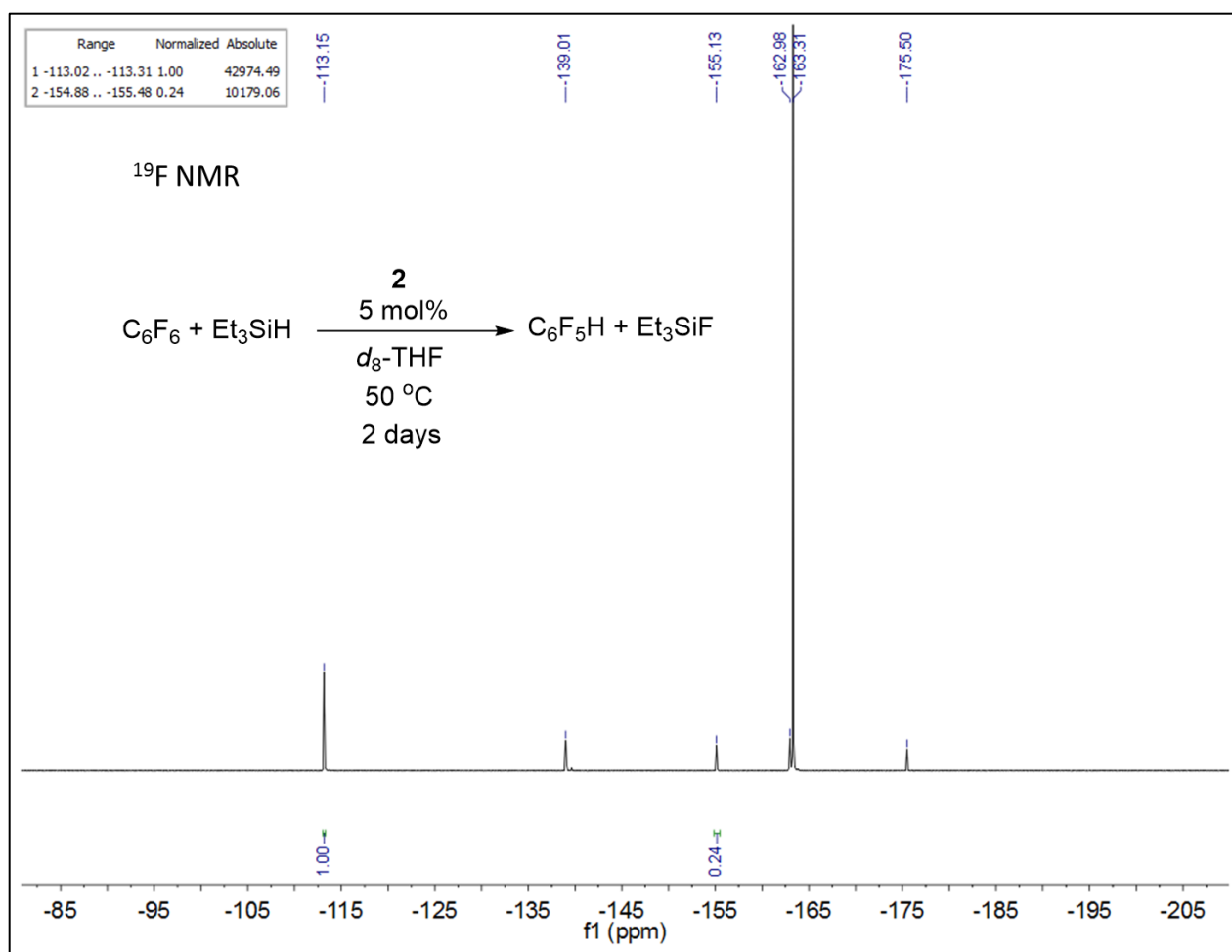


Figure S18: ¹⁹F NMR spectrum for the final time point at 2 days for the catalytic monodefluorination of C₆F₆ in the presence of Et₃SiH using **2** as the catalyst at 50 °C in *d*₈-THF. A stoichiometric amount of fluorobenzene (C₆H₅F) relative to the initial C₆F₆ and Et₃SiH was used as the internal standard (0.219 M, 0.169 mmol). The ¹⁹F resonance corresponding to the *para* position of pentafluorobenzene (C₆F₅H) at δ -155.1 was used for integration purposes (TON=4.2). A relaxation delay of 50 seconds was used between scans in the ¹⁹F NMR experiment (282 MHz, *d*₈-THF, 25 °C).

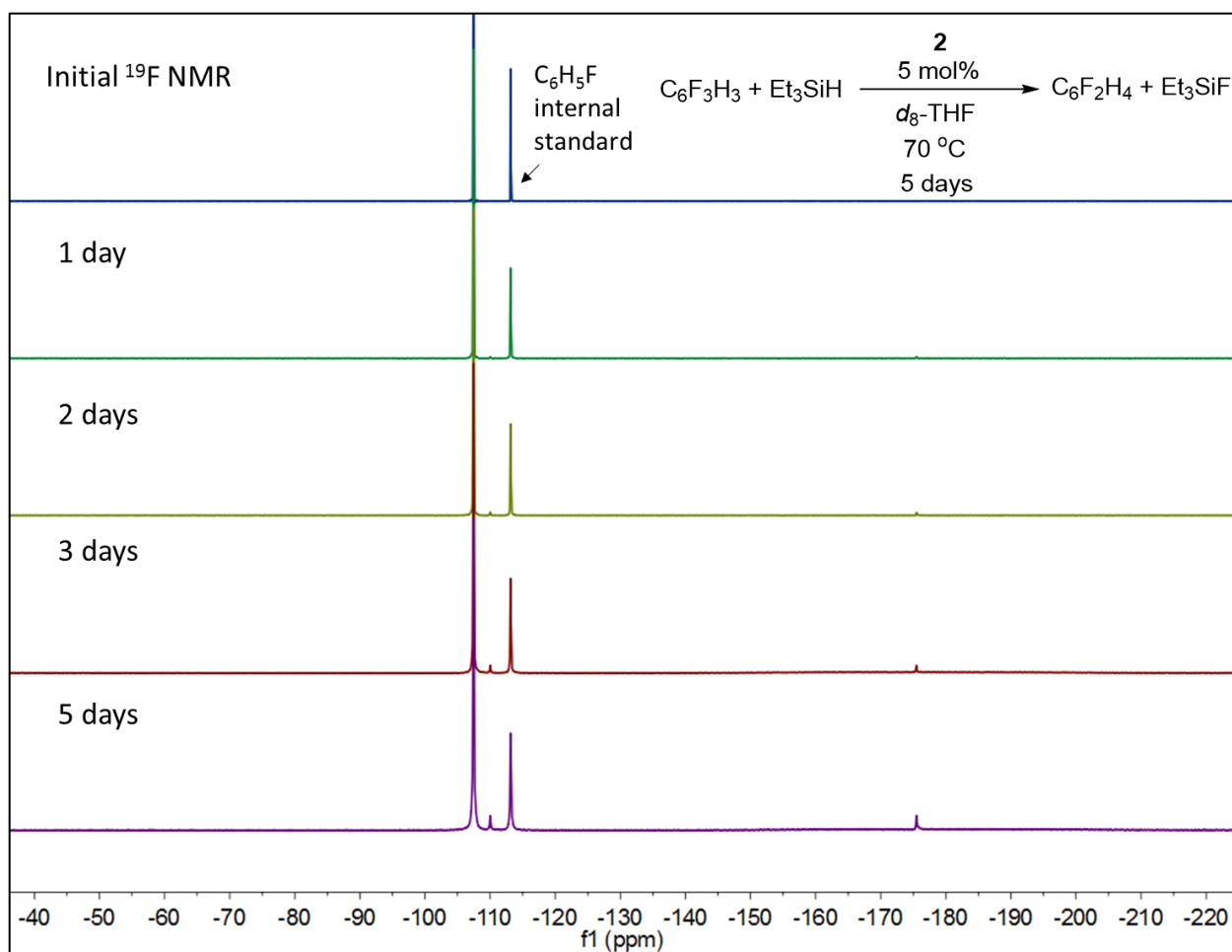


Figure S19: Stacked ^{19}F NMR spectra for the monodefluorination of $\text{C}_6\text{F}_3\text{H}_3$ in the presence of Et_3SiH using **2** as the catalyst at 70°C in $d_8\text{-THF}$. Fluorobenzene ($\text{C}_6\text{H}_5\text{F}$) is used as the internal standard. The ^{19}F resonances corresponding to 1,3-difluorobenzene ($\text{C}_6\text{F}_2\text{H}_4$) at $\delta - 110.0$ and fluorotriethylsilane at $\delta - 175.5$ are first observed after 2 days of reactivity. All spectra collected in $d_8\text{-THF}$ at 282 MHz at 25°C .

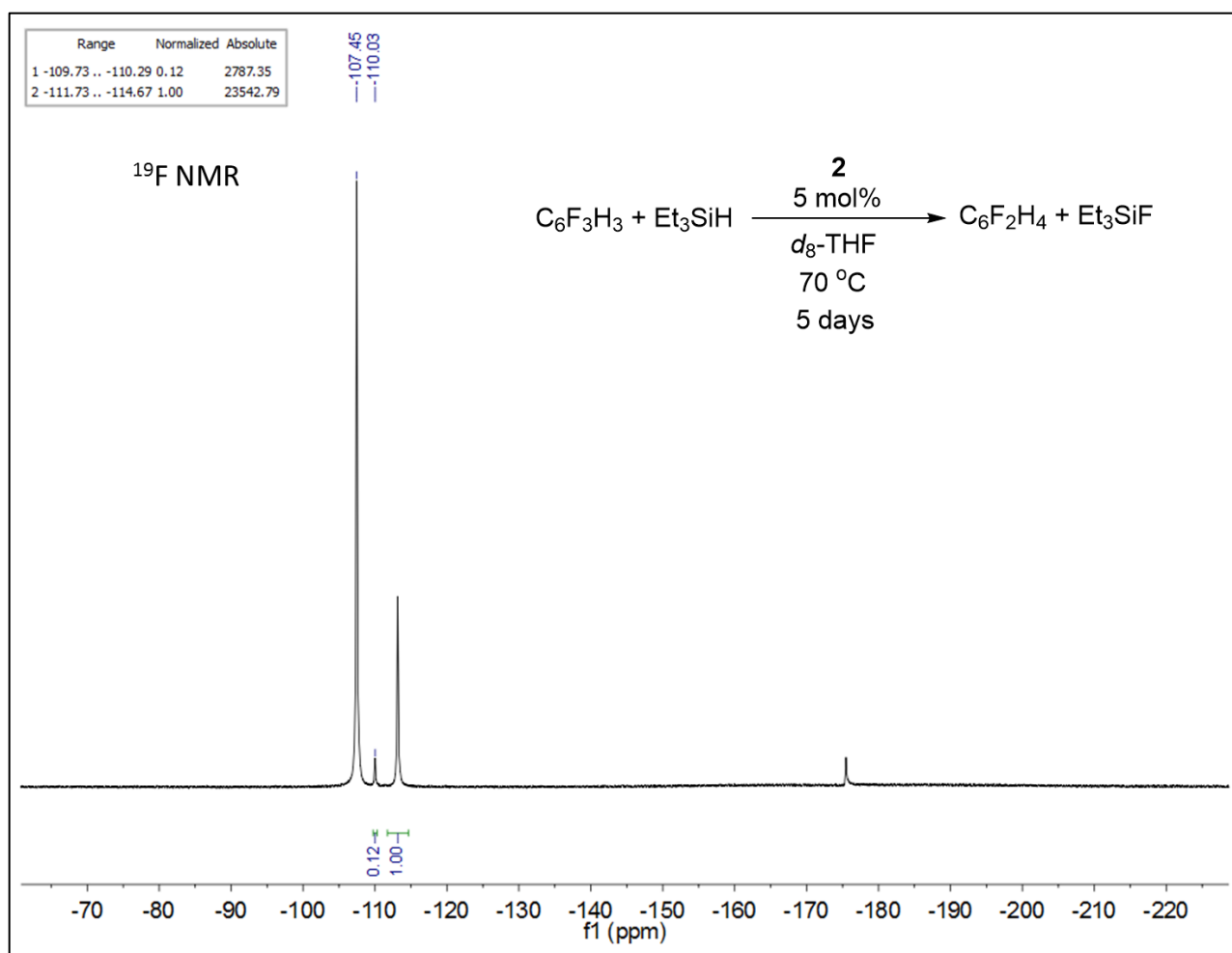


Figure S20: ¹⁹F NMR spectrum for the final time point at 5 days for the monodefluorination of C₆F₃H₃ in the presence of Et₃SiH using **2** as the catalyst at 70 °C in d₈-THF. A stoichiometric amount of fluorobenzene (C₆H₅F) relative to the initial C₆F₃H₃ and Et₃SiH was used as the internal standard (0.546 M, 0.339 mmol). The ¹⁹F resonance corresponding to 1,3-difluorobenzene (C₆F₂H₄) at δ -110.0 was used for integration purposes (TON=1.2). A relaxation delay of 70 seconds was used between scans in the ¹⁹F NMR experiment (282 MHz, d₈-THF, 25 °C).

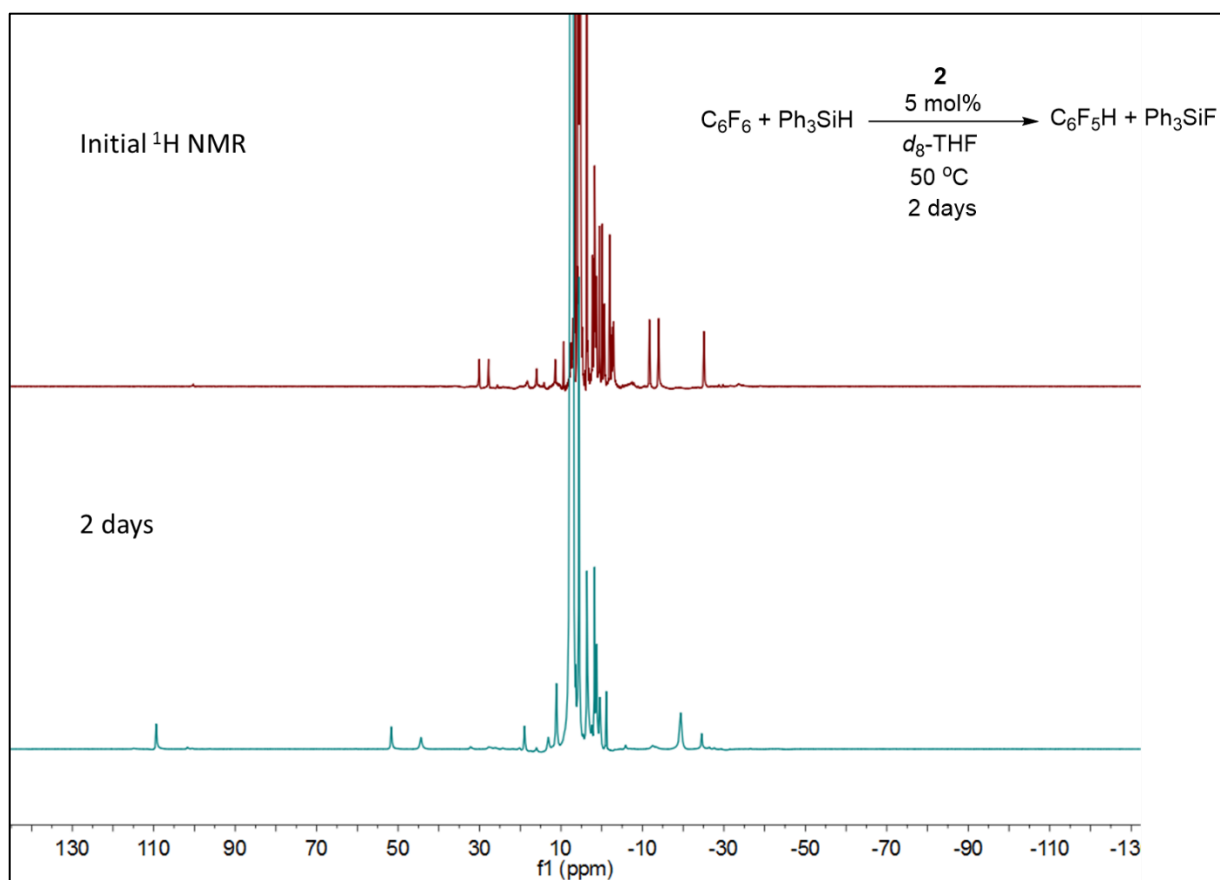


Figure S21: Stacked ^1H NMR spectra for the catalytic monodefluorination of C_6F_6 in the presence of Ph_3SiH using **2** as the catalyst at $50\text{ }^\circ\text{C}$ in $d_8\text{-THF}$. A new paramagnetic species is formed, which is the resting state of the catalyst. All spectra collected in $d_8\text{-THF}$ at 300 MHz at $25\text{ }^\circ\text{C}$.

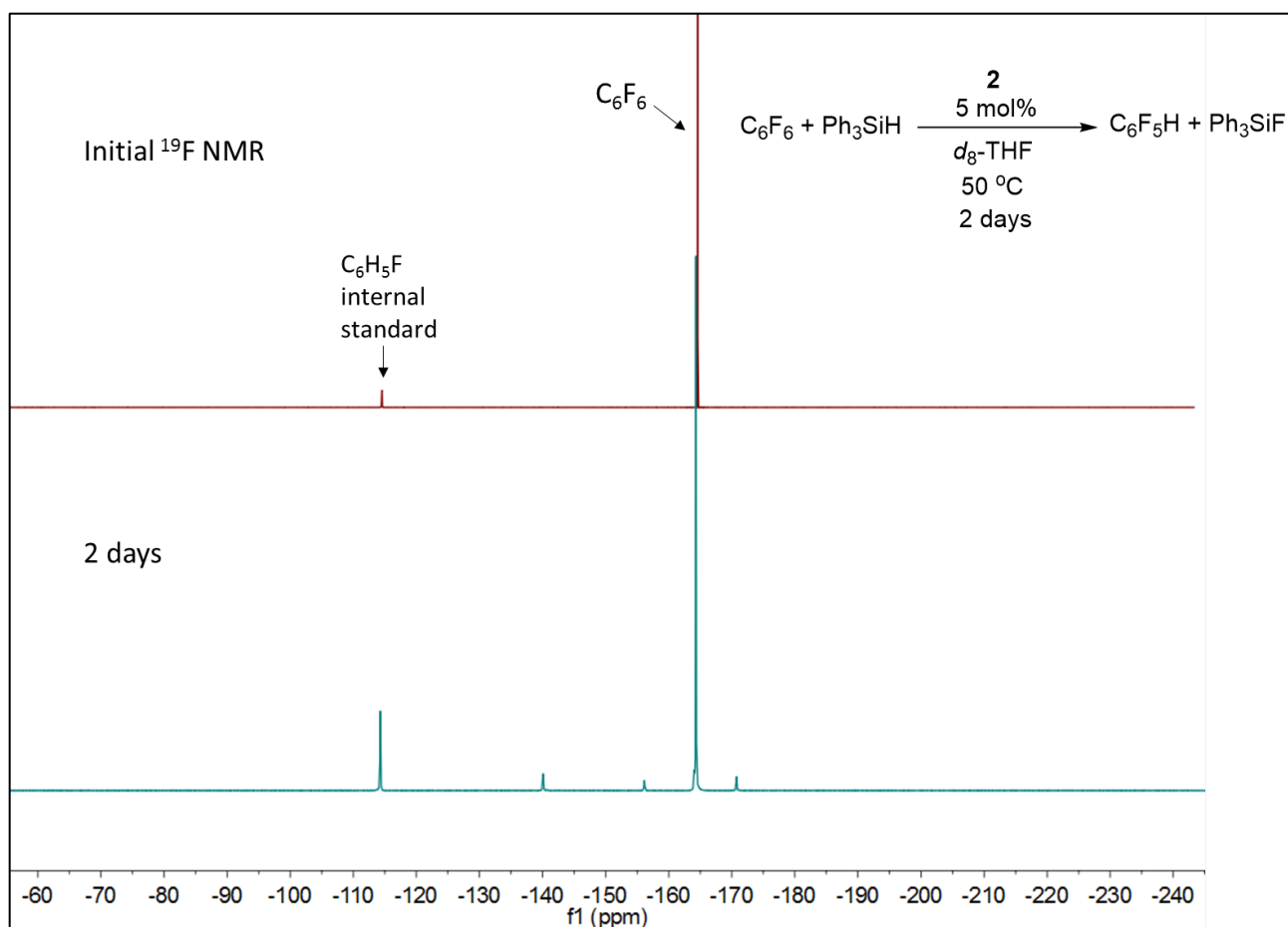


Figure S22: Stacked ^{19}F NMR spectra for the catalytic monodefluorination of C_6F_6 in the presence of Ph_3SiH using **2** as the catalyst at $50\text{ }^\circ\text{C}$ in $d_8\text{-THF}$. Fluorobenzene ($\text{C}_6\text{H}_5\text{F}$) is used as the internal standard. ^{19}F resonances corresponding to pentafluorobenzene ($\text{C}_6\text{F}_5\text{H}$) at δ -139.0, -155.0, and -162.9 and fluorotriphenylsilane at δ -169.6 are observed after 2 days of reactivity. All spectra collected in $d_8\text{-THF}$ at 282 MHz at $25\text{ }^\circ\text{C}$.

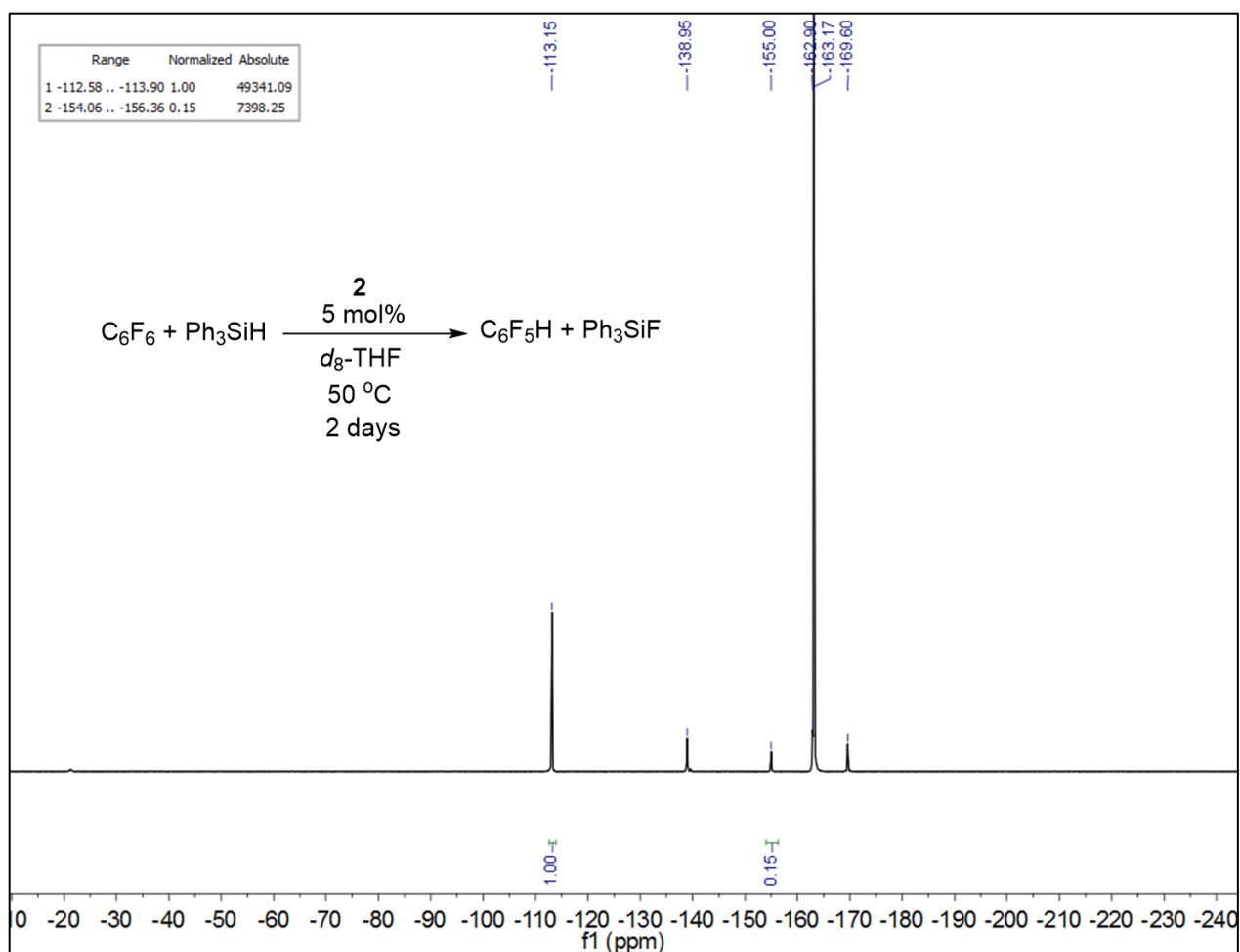


Figure S23: ^{19}F NMR spectrum for the final time point at 2 days for the catalytic monodefluorination of C_6F_6 in the presence of Ph_3SiH using **2** as the catalyst at $50\text{ }^\circ\text{C}$ in $d_8\text{-THF}$. A stoichiometric amount of fluorobenzene ($\text{C}_6\text{H}_5\text{F}$) relative to the initial C_6F_6 and Ph_3SiH was used as the internal standard (0.796 M, 0.440 mmol). The ^{19}F resonance corresponding to the *para* position of pentafluorobenzene ($\text{C}_6\text{F}_5\text{H}$) at δ -155.0 was used for integration purposes (TON=3.0). A relaxation delay of 50 seconds was used between scans in the ^{19}F NMR experiment (282 MHz, $d_8\text{-THF}$, $25\text{ }^\circ\text{C}$).

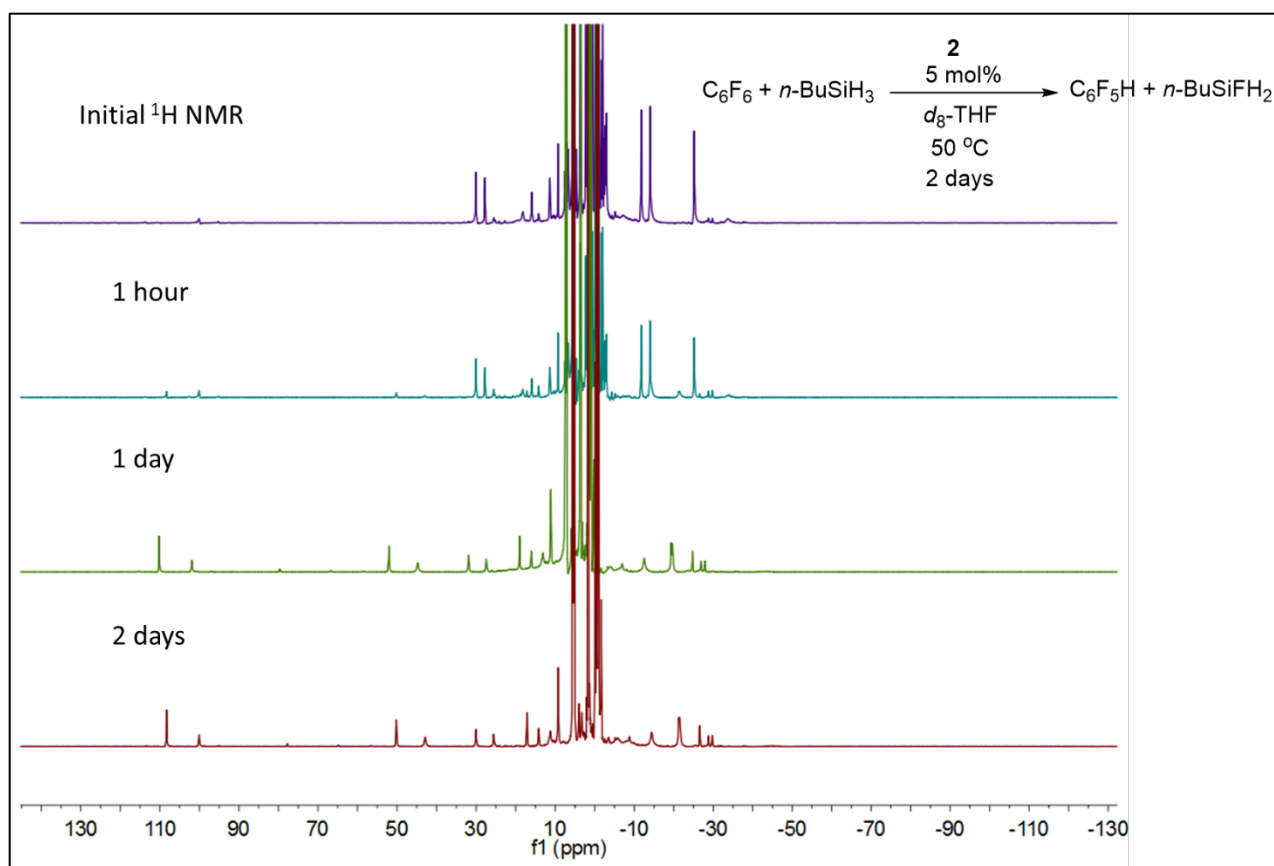


Figure S24: Stacked ^1H NMR spectra for the catalytic monodefluorination of C_6F_6 in the presence of $n\text{-BuSiH}_3$ using **2** as the catalyst at 50°C in $d_8\text{-THF}$. A new paramagnetic species is formed, which is the resting state of the catalyst. All spectra collected in $d_8\text{-THF}$ at 300 MHz at 25°C .

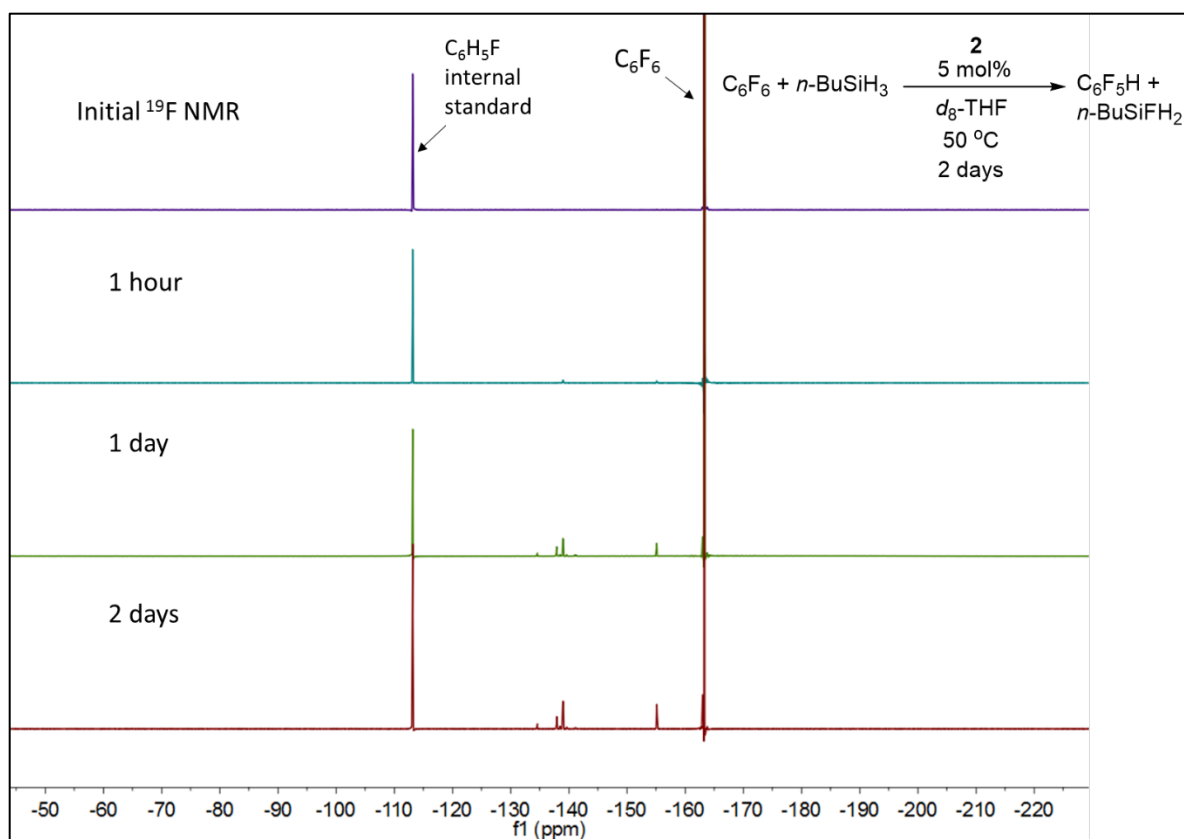


Figure S25: Stacked ^{19}F NMR spectra for the catalytic monodefluorination of C_6F_6 in the presence of $n\text{-BuSiH}_3$ using **2** as the catalyst at 50°C in $d_8\text{-THF}$. Fluorobenzene ($\text{C}_6\text{H}_5\text{F}$) is used as the internal standard. ^{19}F resonances corresponding to pentafluorobenzene ($\text{C}_6\text{F}_5\text{H}$) at δ - 138.9, -155.1, and -163.0 are first observed after 1 day of reactivity. All spectra collected in $d_8\text{-THF}$ at 282 MHz at 25°C .

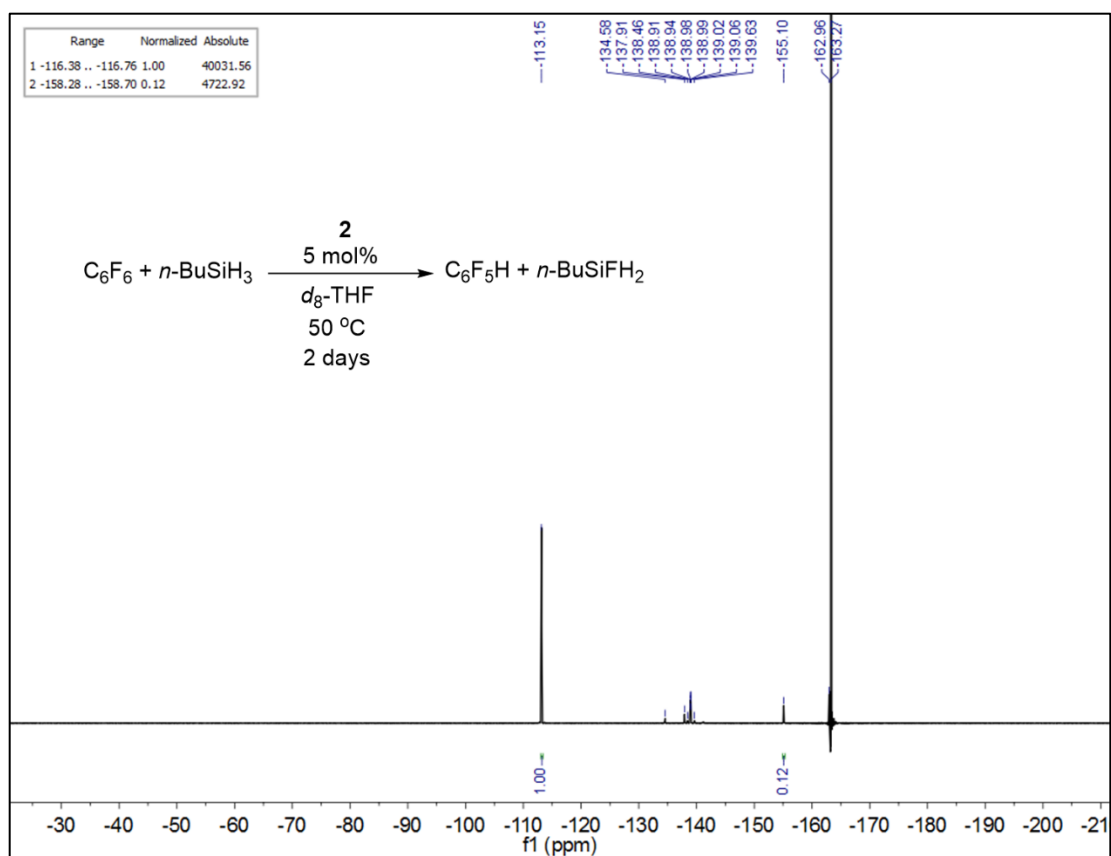


Figure S26: ^{19}F NMR spectrum for the final time point at 2 days for the catalytic monodefluorination of C_6F_6 in the presence of $n\text{-BuSiH}_3$ using **2** as the catalyst at $50\text{ }^\circ\text{C}$ in $d_8\text{-THF}$. A stoichiometric amount of fluorobenzene ($\text{C}_6\text{H}_5\text{F}$) relative to the initial C_6F_6 and $n\text{-BuSiH}_3$ was used as the internal standard (0.576 M, 0.440 mmol). The ^{19}F resonance corresponding to the *para* position of pentafluorobenzene ($\text{C}_6\text{F}_5\text{H}$) at δ -155.1 was used for integration purposes (TON=2.4). A relaxation delay of 50 seconds was used between scans in the ^{19}F NMR experiment (282 MHz, $d_8\text{-THF}$, $25\text{ }^\circ\text{C}$).

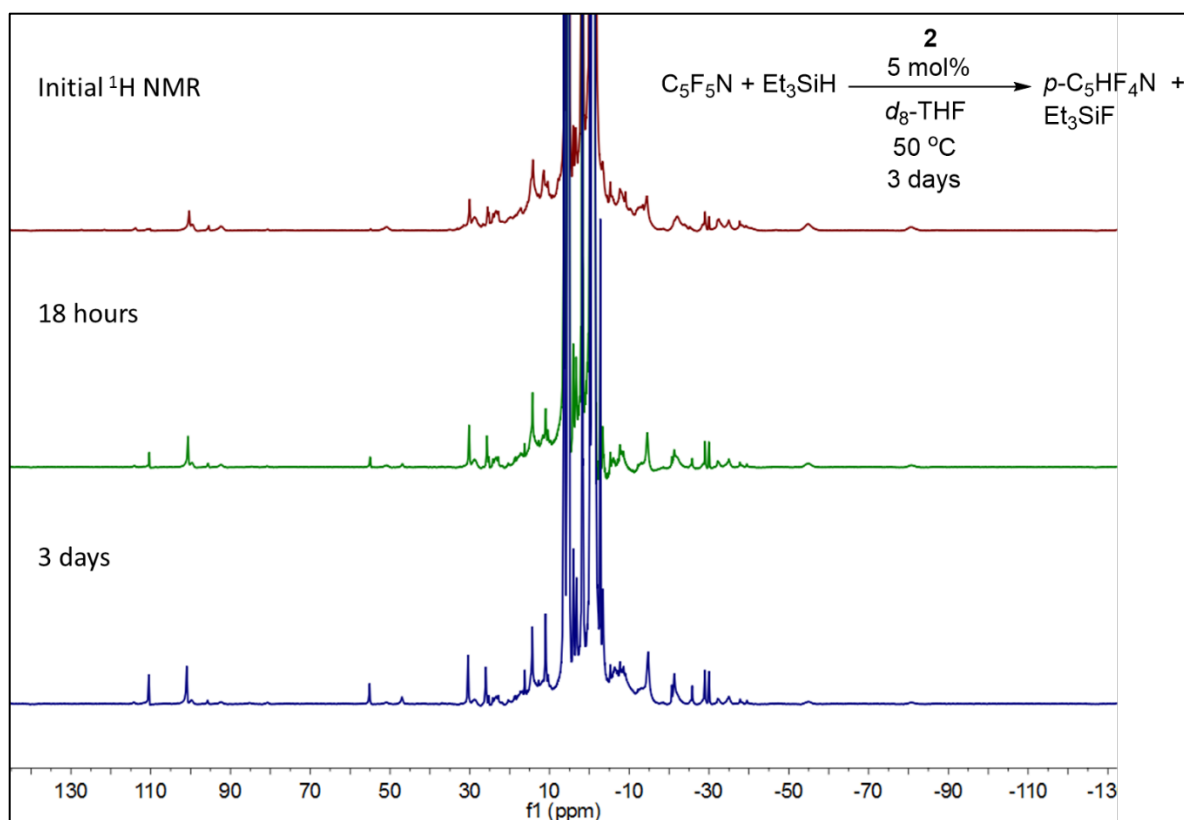


Figure S27: Stacked ^1H NMR spectra for the catalytic monodefluorination of $\text{C}_5\text{F}_5\text{N}$ in the presence of Et_3SiH using **2** as the catalyst at $50\text{ }^\circ\text{C}$ in $d_8\text{-THF}$. A new paramagnetic species is immediately formed from **2** at time point zero. This species is different from the resting state produced during catalysis, as observed at the 18h and 3 day time points. All spectra collected in $d_8\text{-THF}$ at 300 MHz at $25\text{ }^\circ\text{C}$.

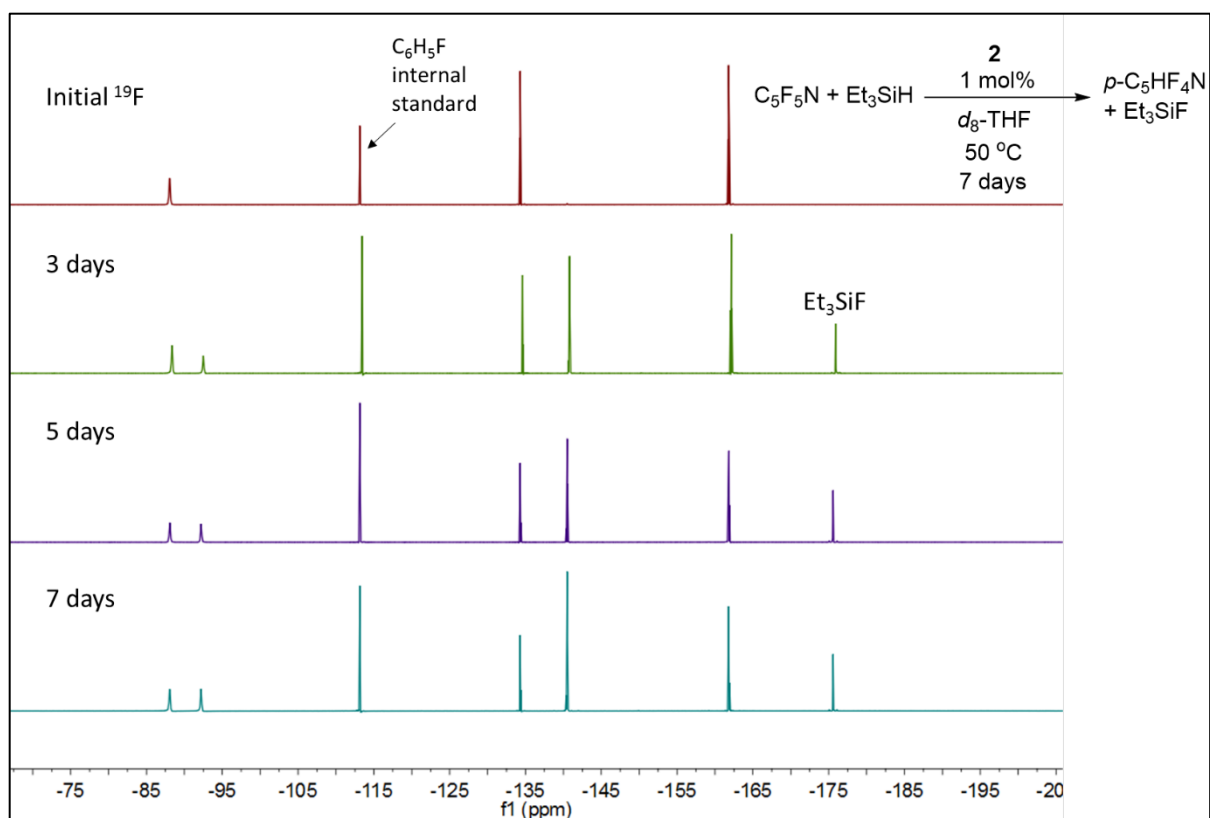


Figure S28: Stacked ^{19}F NMR spectra for the monodefluorination of $\text{C}_5\text{F}_5\text{N}$ in the presence of Et_3SiH using 1 mol% **2** as the catalyst at 50 $^\circ\text{C}$ in $d_8\text{-THF}$. Fluorobenzene ($\text{C}_6\text{H}_5\text{F}$) is used as the internal standard. After a week of reactivity, 50% conversion is obtained as determined by quantitative integration of the Et_3SiF resonance at δ -175.6. All spectra collected in $d_8\text{-THF}$ at 282 MHz at 25 $^\circ\text{C}$.

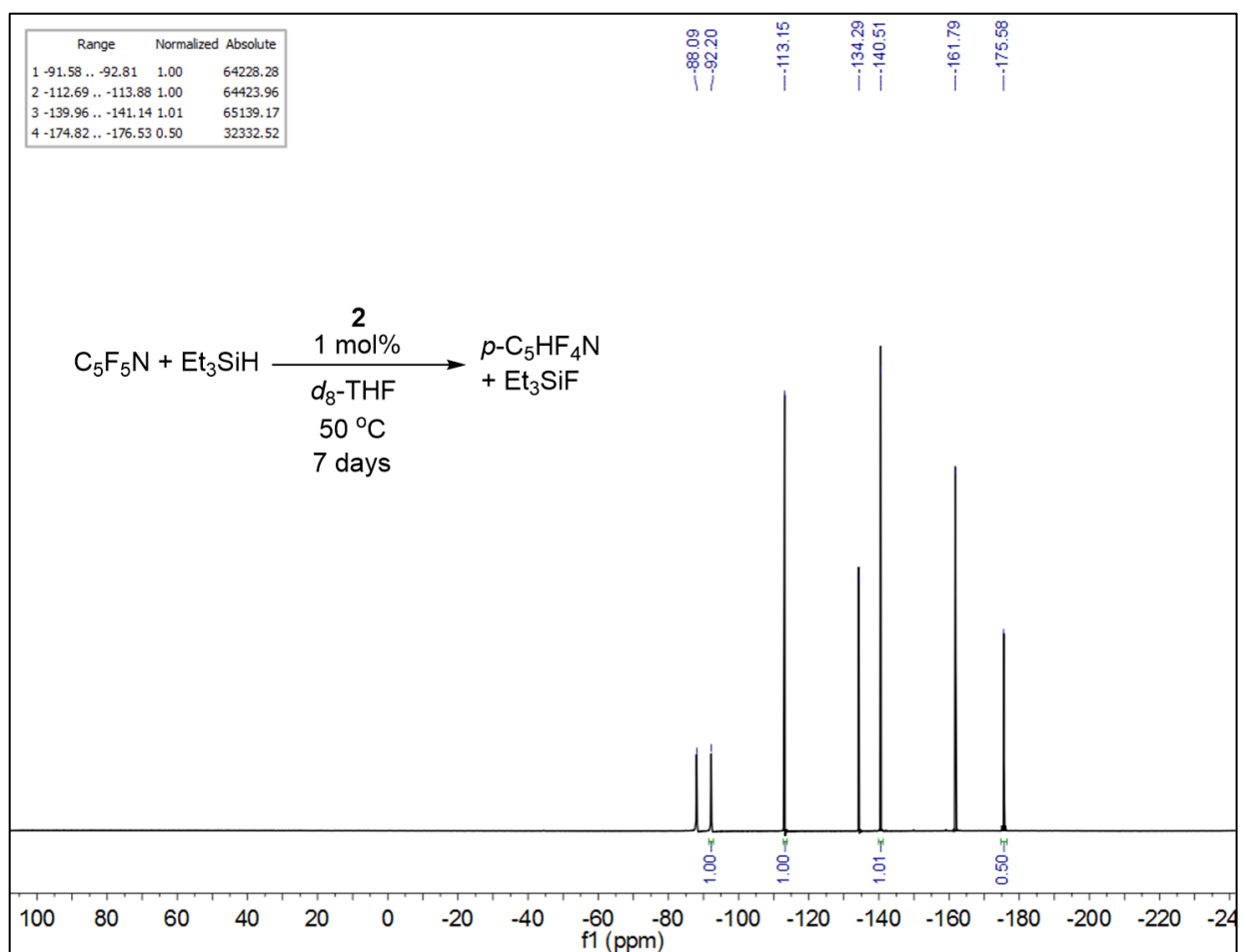


Figure S29: ^{19}F NMR spectrum for the final time point of 7 days in the monodefluorination of $\text{C}_5\text{F}_5\text{N}$ in the presence of Et_3SiH using 1 mol% **2** as the catalyst at $50\text{ }^\circ\text{C}$ in $d_8\text{-THF}$. Fluorobenzene ($\text{C}_6\text{H}_5\text{F}$) at δ -113.2 is used as the internal standard (1.083 M, 0.678 mmol). Integration of the Et_3SiF resonance at δ -175.6 relative to $\text{C}_6\text{H}_5\text{F}$ shows 50% conversion (TON=50). A relaxation delay of 70 seconds was used between each scan in the ^{19}F NMR experiment (282 MHz, $d_8\text{-THF}$, $25\text{ }^\circ\text{C}$).

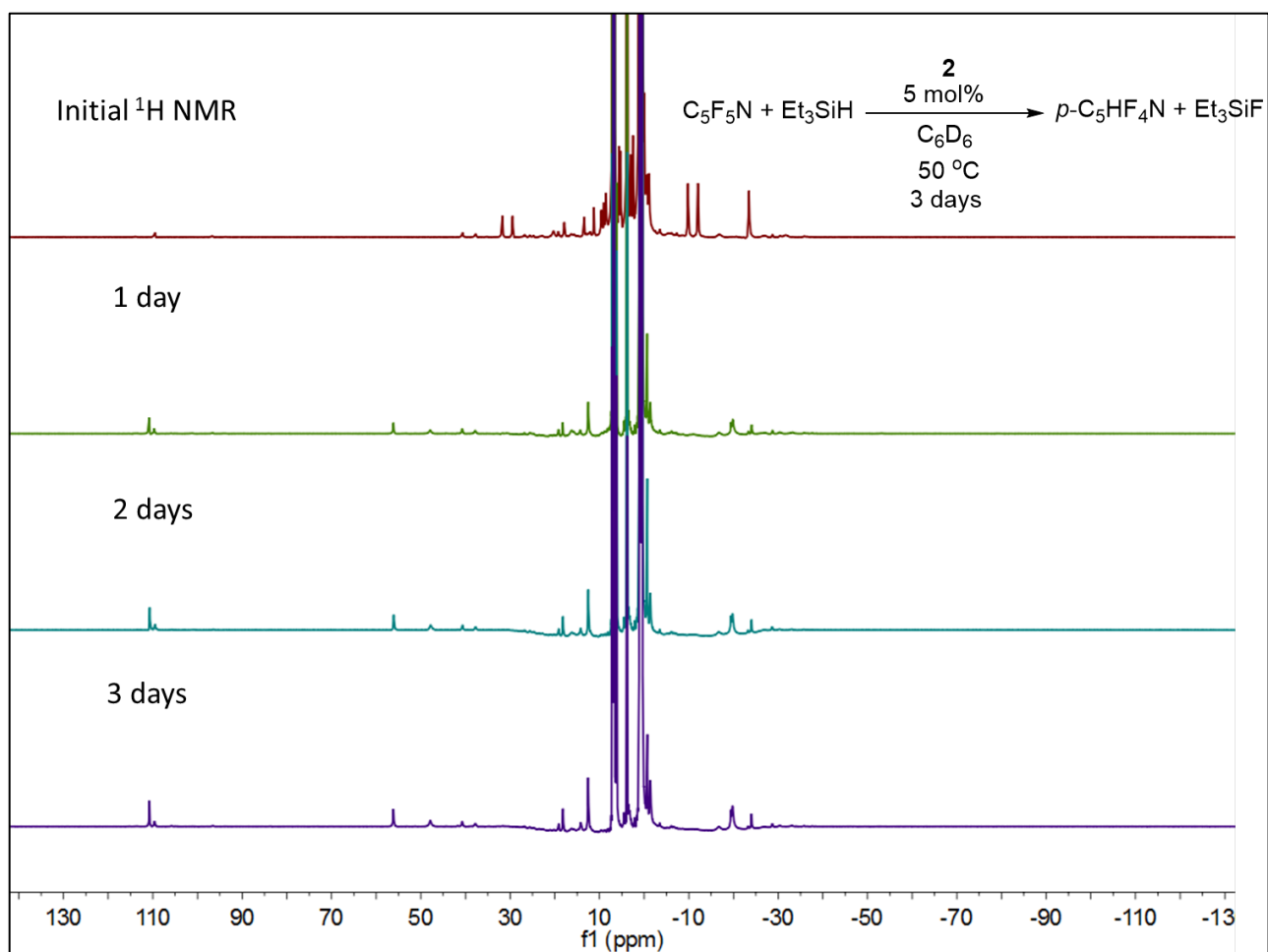


Figure S30: Stacked ^1H NMR spectra for the catalytic monodefluorination of $\text{C}_5\text{F}_5\text{N}$ in the presence of Et_3SiH using **2** as the catalyst at 50°C in d_6 -benzene. A new paramagnetic species is formed from **2** after 1 day of allowing catalysis to proceed. All spectra collected in d_8 -THF at 300 MHz at 25°C .

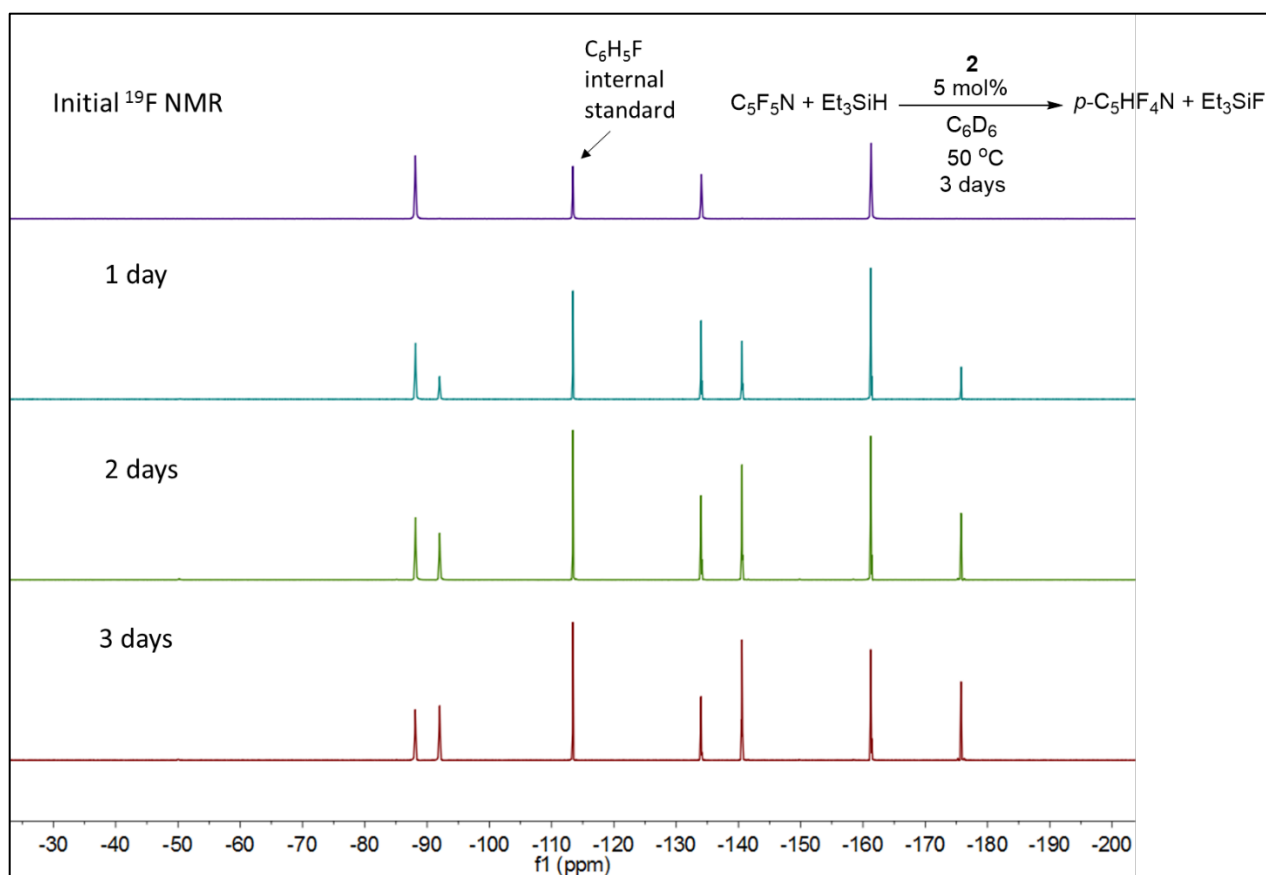


Figure S31: Stacked ^{19}F NMR spectra for the monodefluorination of $\text{C}_5\text{F}_5\text{N}$ in the presence of Et_3SiH using 5 mol% **2** as the catalyst at 50°C in d_6 -benzene. Fluorobenzene ($\text{C}_6\text{H}_5\text{F}$) is used as the internal standard. Conversion is lower compared to when catalysis is performed in d_8 -THF (**Figure S28**). A relaxation delay of 70 seconds was used between each scan in the ^{19}F NMR experiment. All spectra collected in d_6 -benzene at 282 MHz at 25°C .

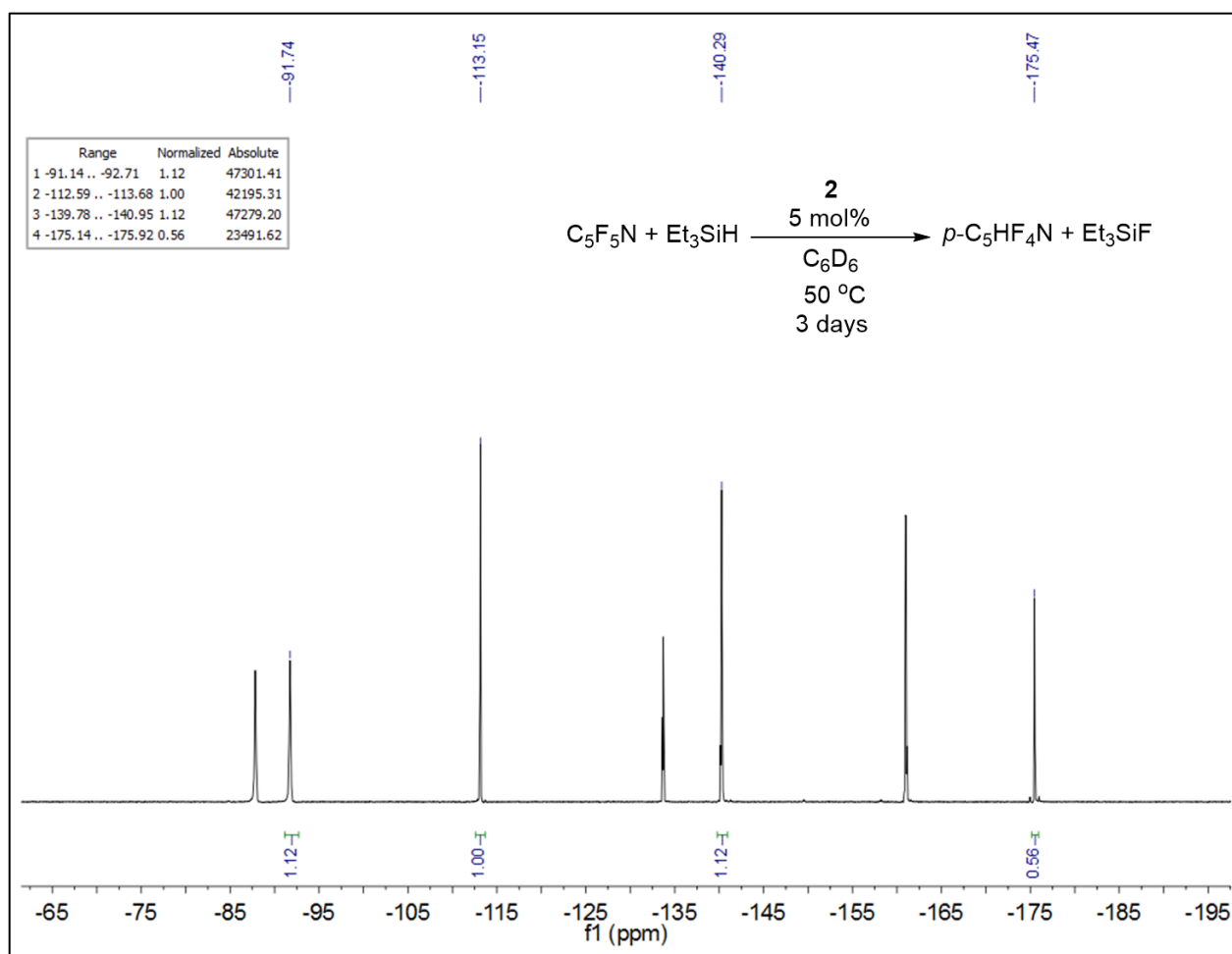


Figure S32: ¹⁹F NMR spectrum for the final time point after 3 days for the monodefluorination of C₅F₅N in the presence of Et₃SiH using 5 mol% **2** as the catalyst at 50 °C in *d*₆-benzene. Fluorobenzene (C₆H₅F) at δ -113.2 is used as the internal standard (0.703 M, 0.372 mmol). Integration of the Et₃SiF resonance at δ -175.6 relative to C₆H₅F shows 56% conversion (TON=11.2). A relaxation delay of 70 seconds was used between each scan in the ¹⁹F NMR experiment (282 MHz, *d*₈-THF, 25 °C).

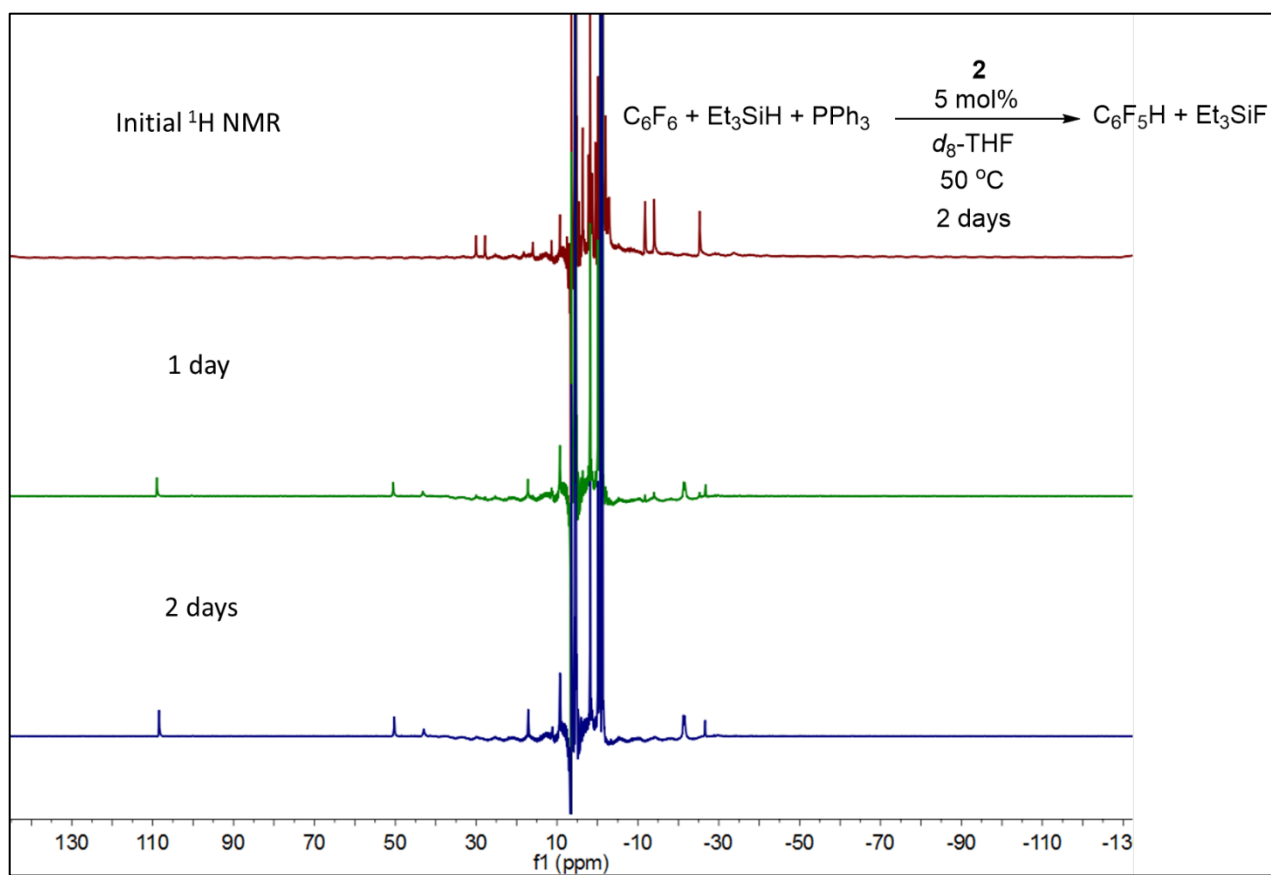


Figure S33: Stacked ^1H NMR spectra for the catalytic monodefluorination of C_6F_6 in the presence of Et_3SiH and PPh_3 using **2** as the catalyst at $50\text{ }^\circ\text{C}$ in $d_8\text{-THF}$. A new paramagnetic species is formed from **2** after 1 day of allowing catalysis to proceed, though this species has the same chemical shifts as the iron containing resting state when catalysis is performed in the absence of PPh_3 . All spectra collected in $d_8\text{-THF}$ at 300 MHz at $25\text{ }^\circ\text{C}$.

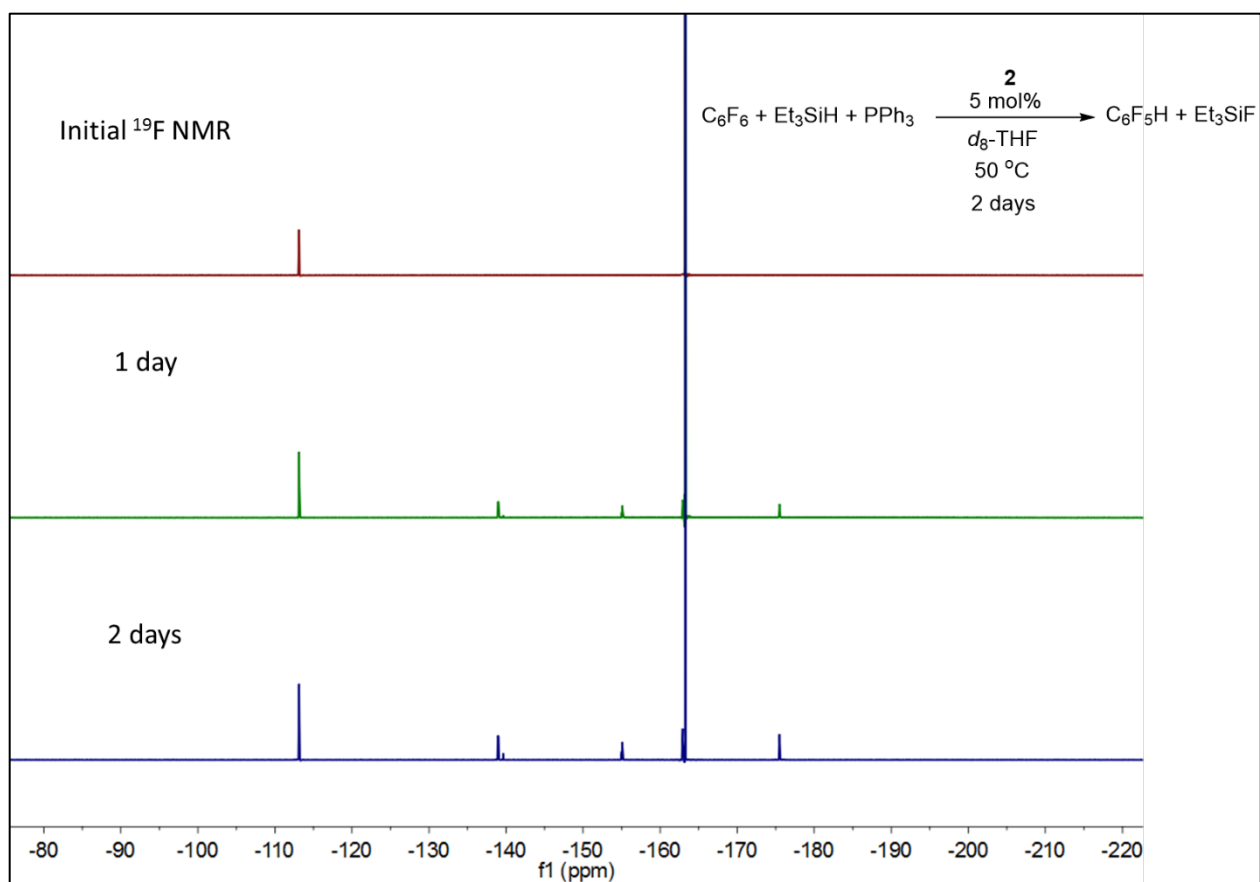


Figure S34: Stacked ^{19}F NMR spectra for the monodefluorination of C_6F_6 in the presence of Et_3SiH and PPh_3 using 5 mol% **2** as the catalyst at 50 $^\circ\text{C}$ in d_8 -THF. Fluorobenzene ($\text{C}_6\text{H}_5\text{F}$) is used as the internal standard. All spectra collected in d_6 -benzene at 282 MHz at 25 $^\circ\text{C}$.

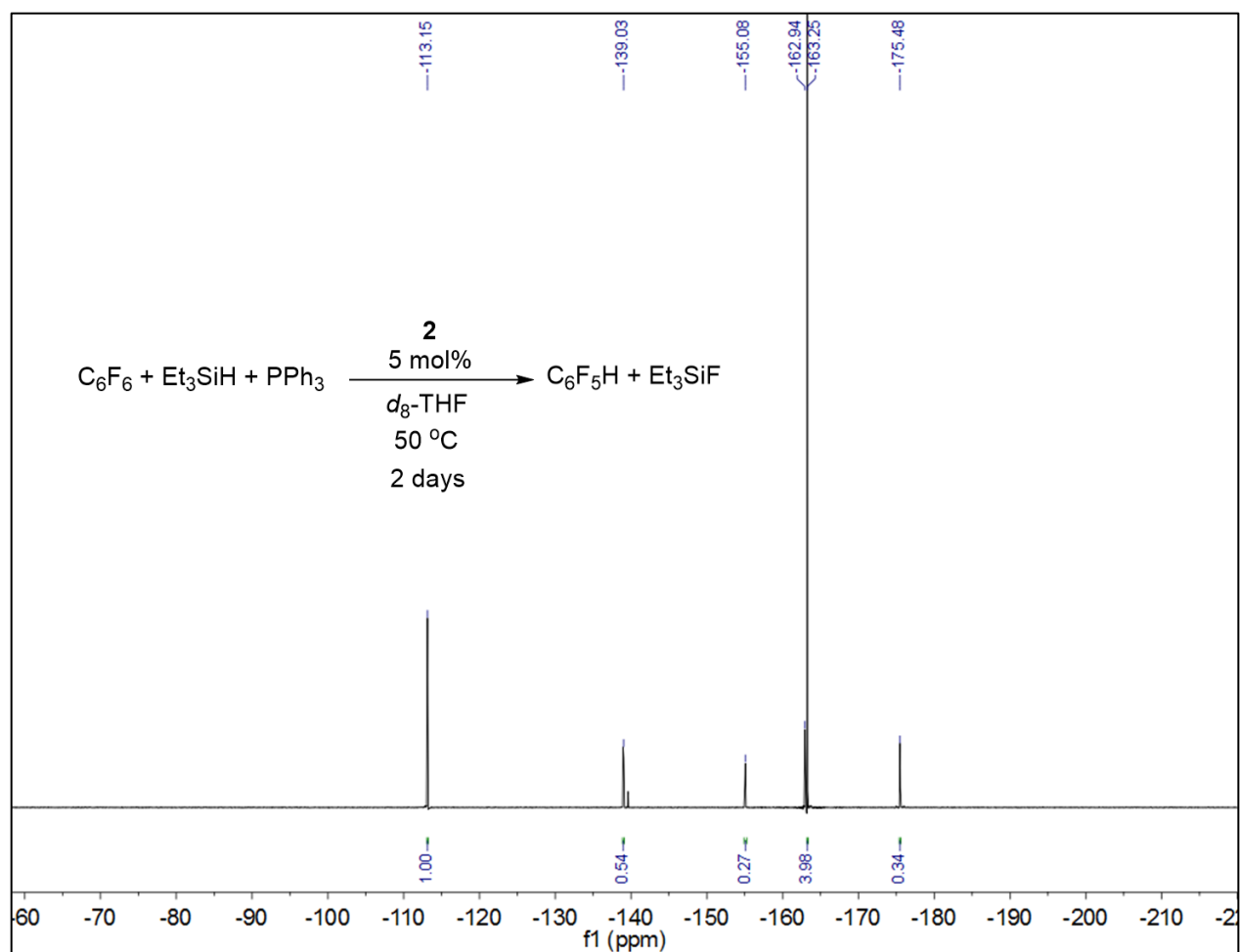


Figure S35: ^{19}F NMR spectrum for the final time point after 2 days for the monodefluorination of C_6F_6 in the presence of Et_3SiH and PPh_3 using 5 mol% **2** as the catalyst at 50 $^\circ\text{C}$ in $d_8\text{-THF}$. Fluorobenzene ($\text{C}_6\text{H}_5\text{F}$) at δ -113.2 is used as the internal standard (0.469 M, 0.203 mmol). The ^{19}F resonance corresponding to the *para* position of pentafluorobenzene ($\text{C}_6\text{F}_5\text{H}$) at δ -155.1 was used for integration purposes (TON=5.4). A relaxation delay of 50 seconds was used between scans in the ^{19}F NMR experiment (282 MHz, $d_8\text{-THF}$, 25 $^\circ\text{C}$).

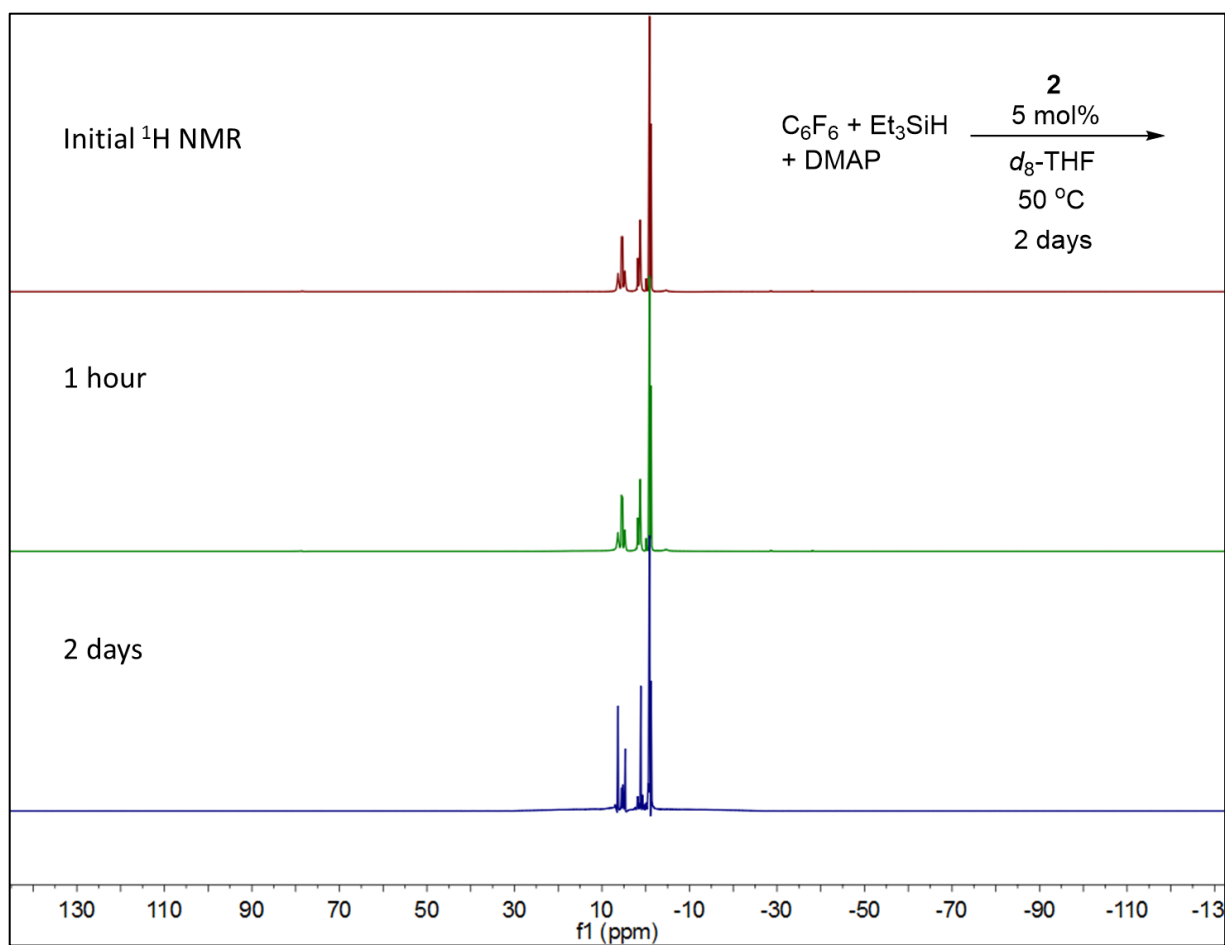


Figure S36: Stacked ^1H NMR spectra for the attempted monodefluorination of C_6F_6 in the presence of Et_3SiH and 4-(dimethylamino)pyridine (DMAP) using 5 mol% **2** at 50 °C in d_8 -THF. A new species is immediately formed from the coordination of DMAP to **2**. All spectra collected in d_8 -THF at 300 MHz at 25 °C.

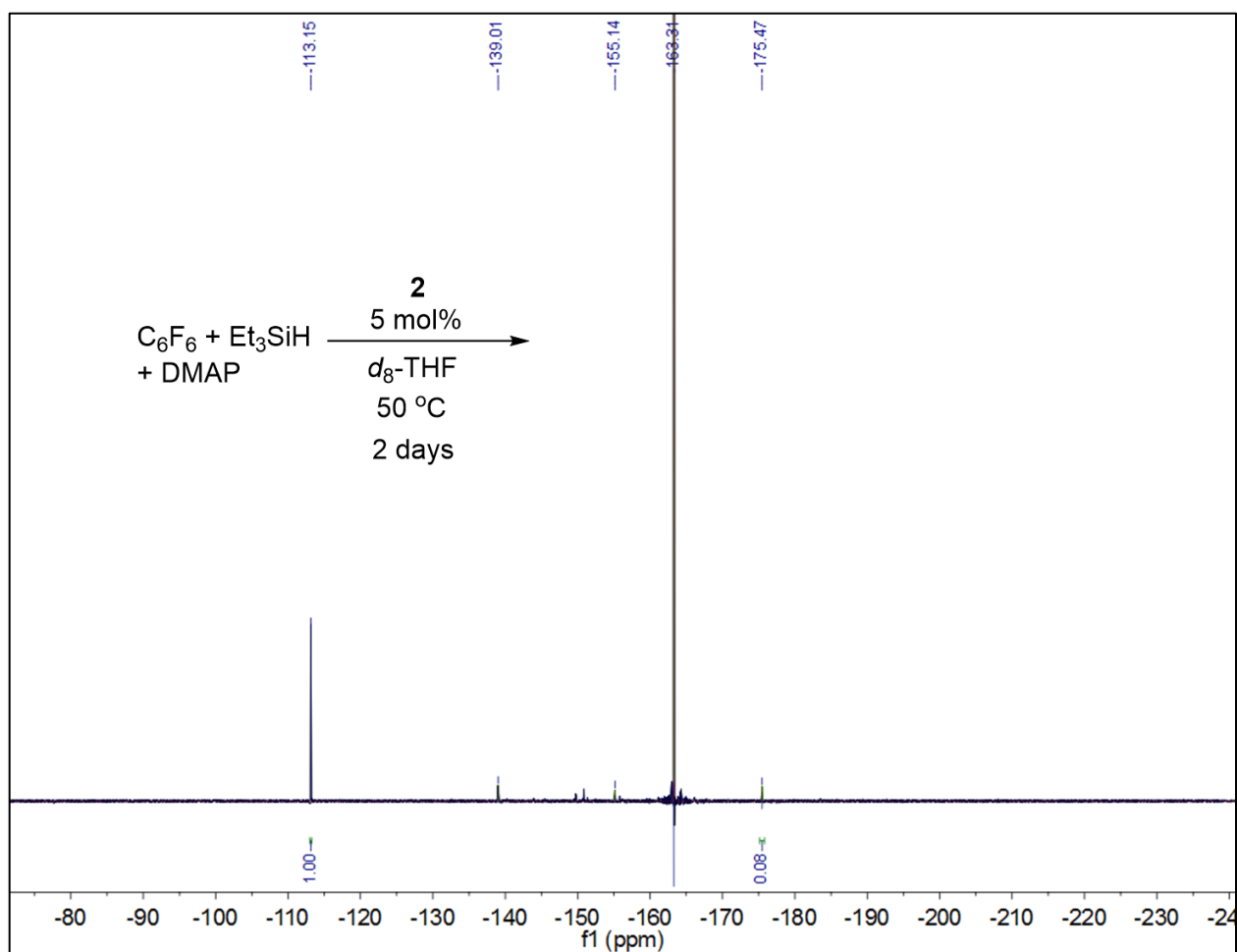


Figure S37: ^{19}F NMR spectrum for the final time point after 2 days for the attempted monodefluorination of C_6F_6 in the presence of Et_3SiH and 4-(dimethylamino)pyridine using 5 mol% **2** at 50 $^\circ\text{C}$ in d_8 -THF. Fluorobenzene ($\text{C}_6\text{H}_5\text{F}$) at δ -113.2 is used as the internal standard (0.462 M, 0.237 mmol). Negligible amounts of the defluorinated product $\text{C}_6\text{F}_5\text{H}$ were formed (282 MHz, d_8 -THF, 25 $^\circ\text{C}$).

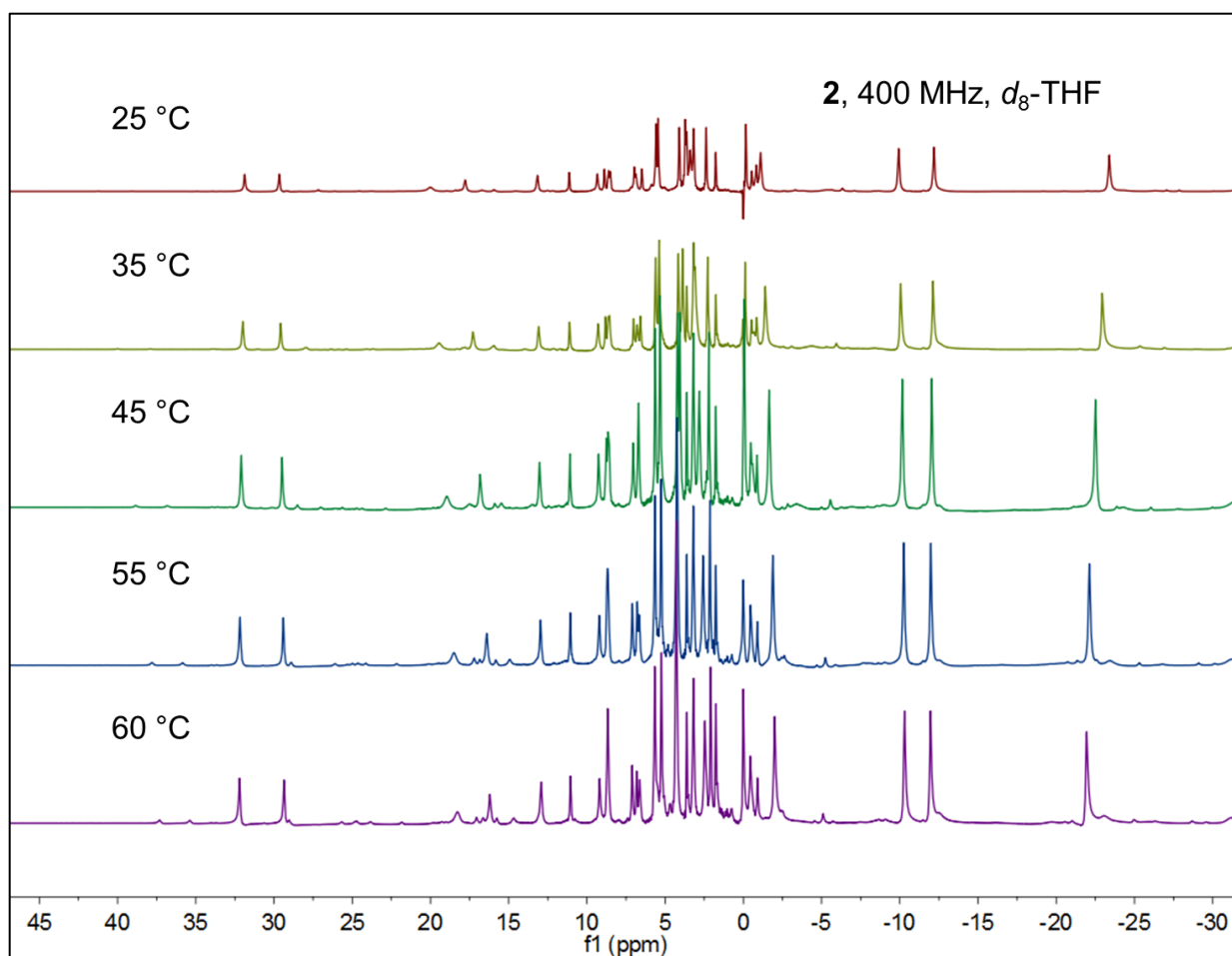


Figure S38: Stacked variable temperature for a *d*₈-THF solution of the dimeric iron hydride **2**. There is not an appreciable difference in the spectra across the various temperatures recorded (see **Figure S39** for a more detailed perspective).

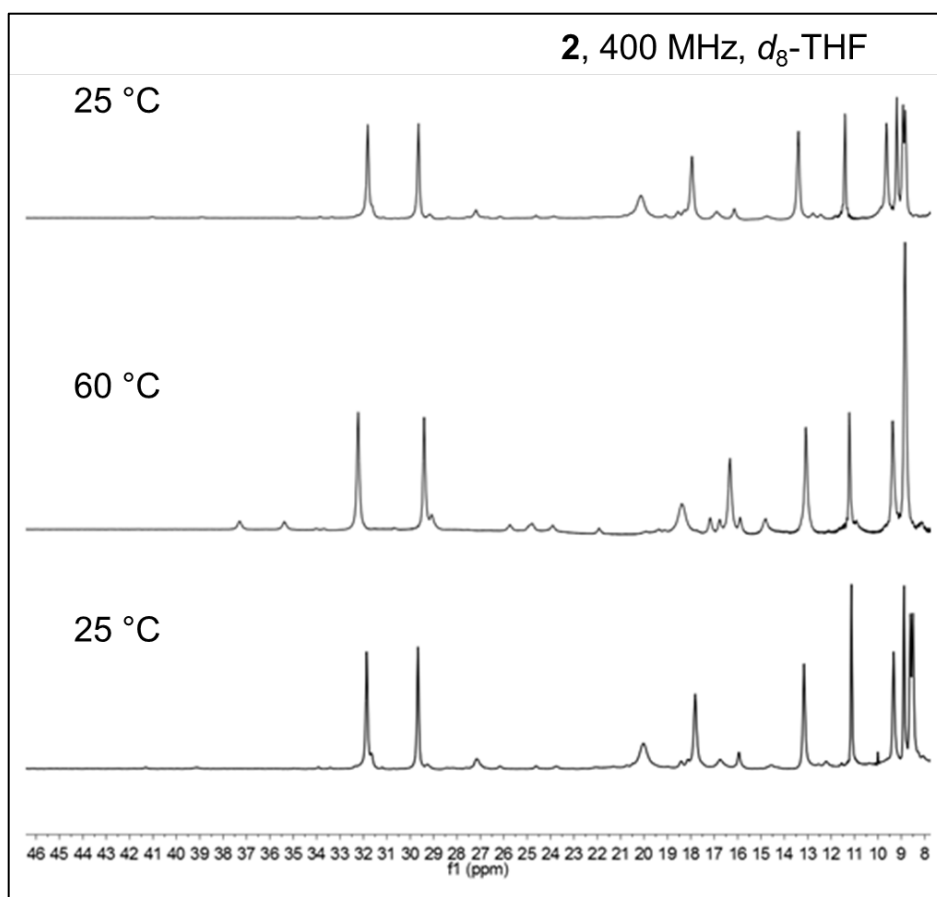


Figure S39: Stacked variable temperature for a *d*₈-THF solution of the dimeric iron hydride **2**. This zoomed-in region shows a new set of resonances that appear at δ 37.3 and 35.4 at 60 °C. These same signals disappear upon cooling the NMR sample to 25 °C. The reversibility of signal appearance/disappearance gives support to the hypothesis that increased temperatures cause a shift in the dimer/monomer equilibrium of **2** to shift to slight monomer production at elevated temperature.

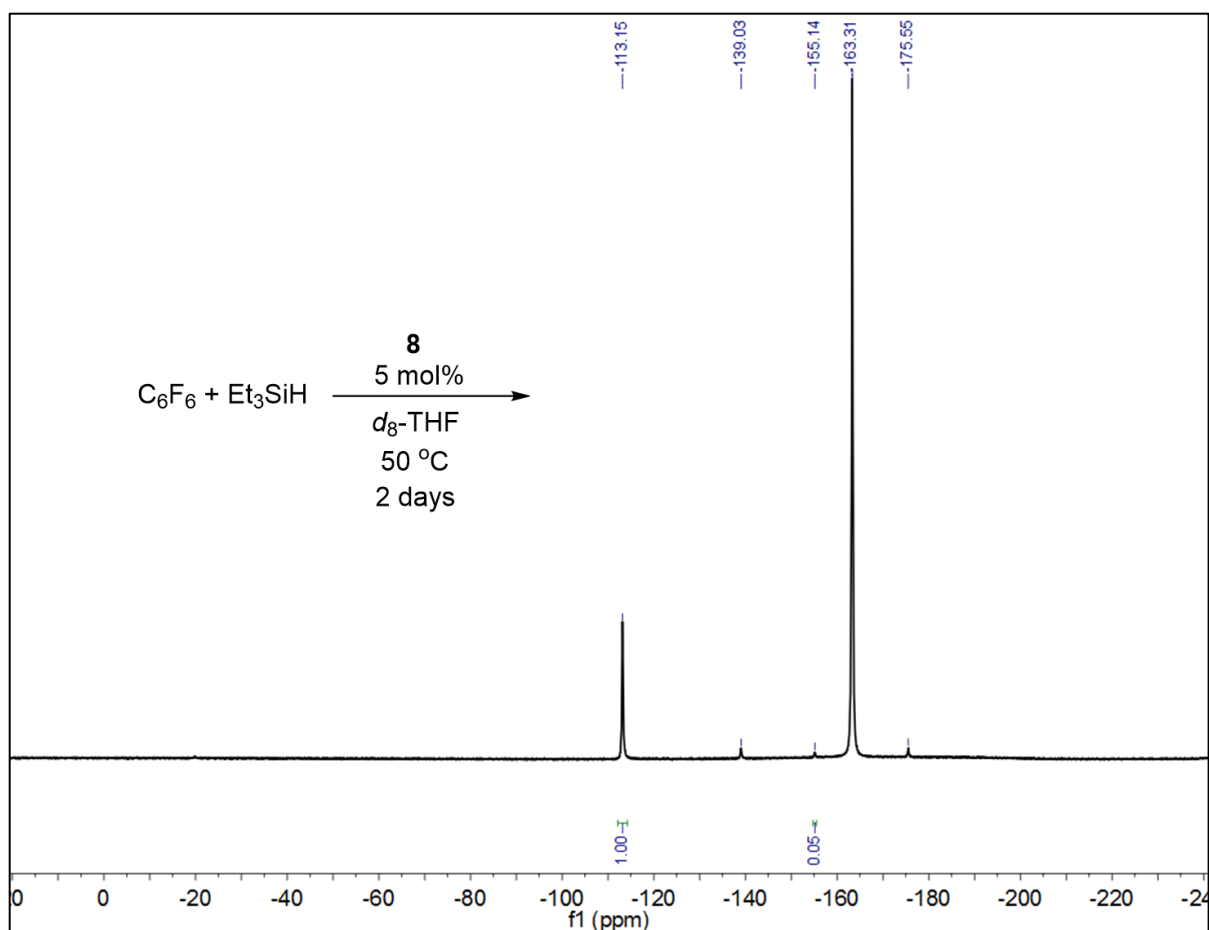


Figure S40: ¹⁹F NMR spectrum for the final time point after 2 days for the attempted monodefluorination of C₆F₆ in the presence of Et₃SiH using 5 mol% **8** at 50 °C in *d*₈-THF. Fluorobenzene (C₆H₅F) at δ -113.2 is used as the internal standard (0.462 M, 0.295 mmol). The ¹⁹F resonance corresponding to the *para* position of pentafluorobenzene (C₆F₅H) at δ -155.1 was used for integration purposes (TON=0.8). A relaxation delay of 50 seconds was used between scans in the ¹⁹F NMR experiment (282 MHz, *d*₈-THF, 25 °C).

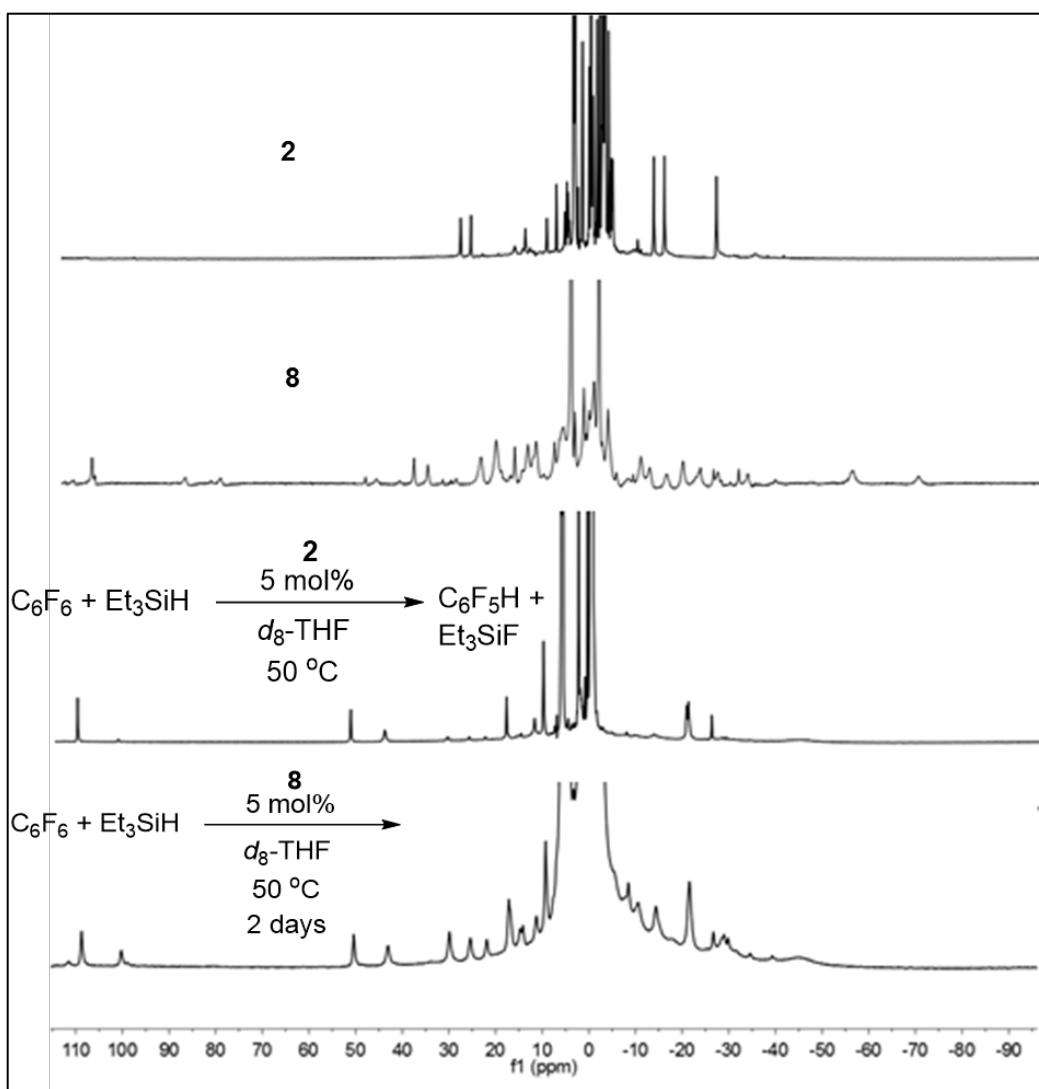


Figure S41: A comparison of the ^1H NMR spectra for **2**, **8**, and the final time points for the HDF catalytic runs using **2** and **8** as precatalysts. The resting state during catalysis is not the hydride species **2** or the fluoride species **8**. All spectra collected in d_8 -THF at 300 MHz at 25 $^\circ\text{C}$.

Additional Kinetic Data

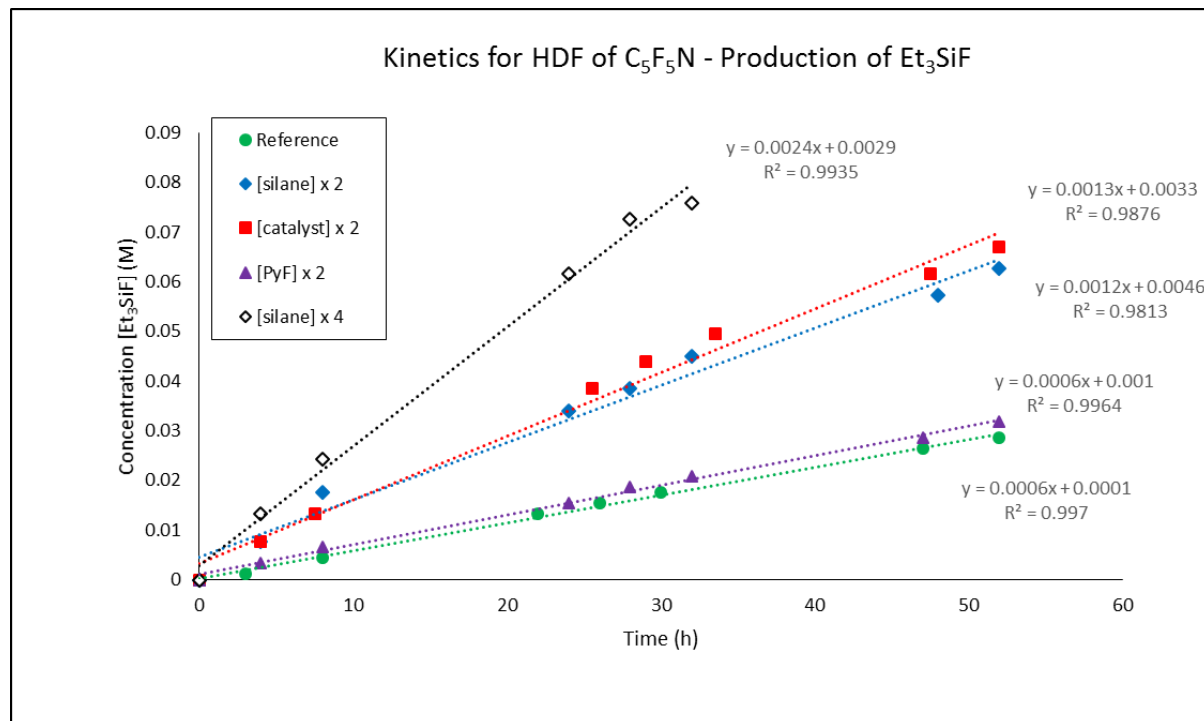


Figure S42: Kinetic evaluation for the production of Et_3SiF during the hydrodefluorination of pentafluoropyridine. The trials shown in the above figure are from the same conditions outlined in the main text (reference: $[silane]=[PyF]=0.11$ M, $[Fe]=5.5 \times 10^{-3}$ M using d_8 -THF at $50^\circ C$).